Biedermann Andrea Regina (Orcid ID: 0000-0001-9819-6969)

Jackson Mike (Orcid ID: 0000-0003-4778-7157)

Bilardello Dario (Orcid ID: 0000-0002-6756-5677)

Feinberg Joshua, M. (Orcid ID: 0000-0002-5845-9848)

Anisotropy of full and partial anhysteretic remanence across different rock types: 2. Coercivity-dependence of remanence anisotropy

Andrea R. Biedermann[1,2], Mike Jackson[1], Dario Bilardello[1], Joshua M. Feinberg[1]

[1] Institute for Rock Magnetism, University of Minnesota, 116 Church St SE, Minneapolis, MN 55455, USA

[2] Institute of Geological Sciences, University of Bern, Baltzerstrasse 1+3, 3012 Bern, Switzerland

Corresponding author: Andrea Biedermann (andrea.regina.biedermann@gmail.com)

Key Points:

- A(p)ARM tensors, principal directions and anisotropy parameters depend on coercivity
- Fabrics of grain sub-populations can interfere positively or negatively
- Carefully choose and report experimental parameters for AARM determination

Abstract

Magnetic fabrics are powerful tools in structural geology and tectonic studies, because they provide a fast and efficient measurement of mineral alignment, which helps interpret a rock's (de)formation history. The magnetic fabric of remanence-carrying minerals provides useful information when these grains record different deformation stages than the bulk minerals in a rock. When rocks contain several sub-populations of remanence-carrying minerals, each of these potentially displays a distinct fabric. This can lead to complex remanence anisotropies, being a superposition of all sub-populations' individual anisotropies. Characterization of partial remanence anisotropies has been used to investigate changes in fabric with grain size. However, most studies still report one bulk remanence anisotropy tensor per sample, and it remains to be determined how commonly different populations of remanence-carrying grains reflect different subfabrics. Based on a large sample collection including 93 specimens from different lithologies, we have investigated the coercivity dependence of anisotropy of (partial) anhysteretic remanent magnetization (A(p)ARM). We find that the principal directions, degree and shape of A(p)ARM are generally dependent on the coercivity window used to impart the ARMs. Depending on the carrier minerals and their fabrics, ARM anisotropy can either increase or decrease when the ARMs are applied over larger coercivity windows. Additionally, the coercivity fraction that dominates the AARM anisotropy is not always the coercivity fraction that acquires the strongest mean ARM. This illustrates the complexity of characterizing remanence anisotropy, and highlights the importance of carefully choosing experimental parameters in A(p)ARM determination for both magnetic fabric and anisotropy correction studies.

1 Introduction

Magnetic fabrics are a direct consequence of the crystallographic and shape preferred orientation of minerals in rocks, and thus reflect rock textures. Magnetic fabric measurements are more efficient and cost-effective than other non-magnetic texture methods, and thus are powerful tools in tectonic and geodynamic studies. The information they provide is particularly useful, when magnetic methods are able to distinguish between the fabrics of different mineral sub-populations within a rock, which may record different stages of deformation. While anisotropy of magnetic susceptibility (AMS) describes the preferred orientation of all minerals in an integrated way, anisotropy of remanence captures the fabrics of remanence-carrying ferromagnetic (*sensu lato*) grains only [*Borradaile and Jackson*, 2010; *Jackson and Tauxe*, 1991]. Remanence anisotropy can be described e.g. by anisotropy of anhysteretic remanent magnetization (AARM) [*McCabe et al.*, 1985], anisotropy of isothermal remanent magnetization (AIRM) [*Stephenson et al.*, 1986], or anisotropy of thermal remanent magnetization (ATRM) [*Cogné*, 1987]. This study will focus on AARM and its coercivity dependence. AARM is frequently used to describe magnetite fabrics, and to determine whether magnetite influences the AMS, and is considered the best room-temperature equivalent of the anisotropy of a natural thermomagnetic remanence [*Potter*, 2004].

1.1 Previous work on AARMs

The minerals contributing to or dominating the AMS or AARM are often different [*Borradaile and Lagroix*, 2000; 2001; *Borradaile et al.*, 1998; *Borradaile et al.*, 1999a; *Borradaile et al.*, 2010; *Chadima et al.*, 2006; *Hirt et al.*, 2014; *Issachar et al.*, 2015; *Lagroix and Borradaile*, 2000a; *Li and Kodama*, 2005; *Oliva-Urcia et al.*, 2009; *Pignotta and Benn*,

1999; *Sagnotti et al.*, 1998; *Viegas et al.*, 2013]. *McCabe et al.* [1985] suggested the use of AARM as a complementary technique to AMS, because the former enhances the contribution of stable single-domain (SD) and pseudo-single-domain (PSD) magnetite grains, whereas paramagnetic minerals and soft ferrimagnets like MD magnetite play a larger role for AMS. *Borradaile et al.* [1993] describe magnetic fabrics in a high-strain shear zone in the Canadian Shield, whose AMS is carried by chlorite, biotite, and amphibole, and the AARM by magnetite and pyrrhotite. Similarly, the AMS in Archean metasediments of the Quetico Belt is carried by mica, but the AARM by pyrrhotite [*Werner and Borradaile*, 1996]. Even in magnetite-rich samples with high mean susceptibility, the AMS can be dominated by paramagnetic minerals, if the magnetite has weak anisotropy [*Borradaile*, 1987; *Borradaile et al.*, 1985/86; *Borradaile and Gauthier*, 2003; *Hirt et al.*, 1995; *Hounslow*, 1985; *Rochette*, 1987; *Rochette and Vialon*, 1984; *Rochette et al.*, 1992]. In contrast, remanence anisotropy can be stronger than the AMS when both are carried by the same mineral. However, a nearly isotropic paramagnetic AMS masks the anisotropic remanence contribution to the AMS. This effect is particularly important for low-field AMS studies, in which remanence anisotropy is not measured [*Cogné* 1987; *Fuller*, 1963; *Hrouda*, 2002; *Stephenson et al.* 1986]. In this case, large corrections on paleomagnetic directions and paleointensities may be needed even when the AMS is weak [*Selkin et al.*, 2000]. A comparison of AMS and AARM principal directions, degree and/or shape of the anisotropy allows for a first estimate as to which minerals carry the AMS, and of whether paramagnetic or ferromagnetic minerals are more anisotropic [*Evans et al.*, 2003; *Gaudreau et al.*, 2017; *Johns et al.*, 1992; *Lycka*, 2017]. *Lagroix and Borradaile* [2000b] used AARM measurements to confirm that AMS in mafic silicate single crystals is disturbed by the effects of magnetite inclusions. *Borradaile et al.*, [1999b] even attempted to isolate the paramagnetic/diamagnetic AMS fabric by subtracting proportions of the AARM tensors from the measured AMS, but later conceded that '… because of the different physical response of the same mineral to remanent and induced magnetism […] we cannot simply subtract the accessory-AARM contribution from a sample's AMS to isolate the matrix AMS …' [*Borradaile*, 2001], in agreement with *Hrouda* [2000]. Hence, characterizing magnetic fabrics using both AARM and AMS has several advantages: (1) AARM targets the anisotropy of remanence-carrying minerals specifically, and is more appropriate for correcting paleomagnetic data than AMS, which instead can be dominated by grains not contributing to remanence, such as dia/paramagnetic minerals or multi-domain (MD) magnetite. (2) The potential number of contributing minerals is more limited for AARMs than for AMS, which may facilitate structural interpretation. (3) Interpretation of AMS is sometimes complicated by the presence of inverse fabrics carried by single-domain (SD) magnetite, which is not an issue for remanence anisotropy [*Stephenson et al.*, 1986]. The latter likely explains why AMS and AARM tensors reported to be carried by magnetite sometimes are coaxial [*Raposo and Gastal*, 2009; *Raposo et al.*, 2007; *Raposo et al.*, 2012], or sometimes display interchanged axes [*Calvin et al.*, 2017; *Kon et al.*, 2017; *Raposo and D'Agrella-Filho*, 2000; *Raposo et al.*, 2014; *Soriano et al.*, 2016].

One useful consequence of different carriers for AMS and AARM is that they can often record different stages of deformation. In the Sassamansville diabase, Pennsylvania, USA, primary low-coercivity magnetite dominates the AMS developed during emplacement, while high-coercivity magnetite grown during a subsequent hydrothermal event holds the AARM [*Kodama and Mowery*, 1994]. Similarly, the AARM of the Borrowdale slaty tuff, United Kingdom, is believed to record a different episode of deformation than the AMS [*Nakamura and Borradaile*, 2001]. In the Thomson Formation, MN, USA, AARM has been interpreted to reflect a primary depositional fabric, whereas the AMS, primarily due to chlorite, was overprinted by a later tectonic deformation [*Sun et al.*, 1995]. Similarly, the

AMS in Devonian black shales of Appalachian Plateau relates to vertical compaction whereas the AARM does not [*Hirt et al.*, 1995]. In the Dukla Nappe, Outer Western Carpathians, Poland, the AARM is less sensitive to tectonic overprints than the AMS, indicating that the magnetite grains were less affected by this deformation than the rock-forming paramagnetic minerals [*Kiss et al.*, 2016]. If AMS and AARM fabrics are coaxial, they can either both be carried by the same mineral, e.g. magnetite [*Kissel et al.*, 1998], or by different minerals that record the same deformation [*Biedermann et al.*, 2016; *Yokoyama et al.*, 2012].

AARMs have been successfully measured on apparently undeformed to weakly deformed limestones with weak magnetizations [*Jackson et al.*, 1989b; *Raposo et al.*, 2006], speleothems [*Ponte et al.*, 2017], and coccolith calcite rocks [*Issachar et al.*, 2018]. The degree of AARM can record gradual changes in finite strain, even when the AMS does not [*Housen and van der Pluijm*, 1991]. Furthermore, AARM has been shown to correlate with stress during experimental deformation of synthetic magnetite-bearing calcite sandstones [*Jackson et al.*, 1993], and with strain in syntectonically deformed granites [*Mamtani et al.*, 2011], similar to empirical relationships between AMS degree and strain [*Cogné and Perroud*, 1988; *Hirt et al.*, 1993; *Kligfield et al.*, 1977; *Kligfield et al.*, 1981].

Correlations have been found between AARM and the direction of natural remanent magnetization (NRM), leading to the recommendation to use AARM measurements to identify and correct for inclination shallowing [*Biedermann et al.*, 2017; *Collombat et al.*, 1993; *Gattacceca and Rochette*, 2002; *Hodych and Bijaksana*, 1993; *Kodama*, 2009; *Werner and Borradaile*, 1996]. *Kodama* [1997] states that an AARM based inclination correction technique should be routinely applied to sedimentary paleomagnetic data. AARM-based anisotropy corrections have also been used in archaeomagnetic studies [*Kapper et al.*, 2017; *Stillinger et al.*, 2015], and a paleointensity study on laboratory-deposited sediments [*Molinek and Bilardello*, 2018]. While AMS-derived anisotropy corrections can be successful if the AMS and AARM fabrics are sufficiently similar [*Bijaksana and Hodych*, 1997; *Hodych et al.*, 1999], AMS is generally an inadequate proxy for remanence anisotropy or anisotropy-induced changes in the magnetization vector. *Selkin et al.* [2000] found a strong directional dependence of paleointensity estimates in anorthosites from the Archean Stillwater Complex, with intensity estimates ranging from 17 µT to 55 µT, for a magnetizing field of 25 µT. AARM-based anisotropy corrections yielded correct estimates, but the very weak AMS could not account for this large variation. Being weaker than AARM, AMS has also been considered inadequate to detect paleofield deflections in archeomagnetism [*Borradaile et al.*, 2001; *Tema*, 2009], or extraterrestrial magnetism [*Gattacceca et al.*, 2003]. Even for remanence anisotropy, it is difficult to obtain a reliable inclination correction in the presence of composite fabrics [*Biedermann et al.*, 2019b; *Bilardello and Kodama*, 2009; *Borradaile and Almqvist*, 2008; *Kodama and Dekkers*, 2004].

1.2 Standard approaches to measuring AARM

AARM fabrics are determined by applying a set of directional anhysteretic remanences (ARMs), measuring the remanences in each direction and calculating the tensor that best describes the relationship $\vec{M}_{rem} = \boldsymbol{k_{rem}}\vec{H}$, where $\vec{M}_{rem}$ is the measured ARM, $\vec{H}$ the applied DC field, and $\boldsymbol{k_{rem}}$ the remanence tensor. This tensor can be computed by using the scalar intensity of $\vec{M}_{rem}$ along the direction of the applied field in at least 6 orientations (parallel components $M_{//} = \vec{M} \cdot \vec{H}/|\vec{H}|$), or based on the full vector $\vec{M}_{rem}$ in at least 3 orientations. The latter requires less measurement time, however, the former is a more reliable representation of $\boldsymbol{k_{rem}}$, e.g. due to gyroremanence [*Bilardello and Jackson*, 2014;

Potter, 2004]. Commonly, $\boldsymbol{k_{rem}}$ is computed from imparting ARMs along 9 orientations, but other measurement schemes using 2 to 39 DC field directions have been used (Figure 1a). Some studies report a minimum AARM estimate based on measurements parallel to at least two of the three principal AMS axes [*de Wall and Worm*, 1993; *Nowaczyk*, 2003]. For each direction, ARMs are imparted by subjecting the sample to a weak DC bias field superposed on an alternating field (AF) that decays to zero from a large initial value. The DC field can be turned on throughout the AF decay (ARM), or only for a part of the AF decay (partial ARM, or pARM). Often, DC bias fields are 0.1 mT, or 0.05 mT, where the latter corresponds to the approximate strength of the Earth's magnetic field (Figure 1b). Other bias fields between 0.01 mT to 1 mT have been used, and sometimes the strength of the DC field is not reported. The choice of DC field may have important consequences, because the degree of AARM depends on the DC field [*Bilardello and Jackson*, 2014]. Other experimental variables that may affect AARM fabrics include whether samples are demagnetized between the magnetization steps in different orientations, and what frequencies and decay rates are used for the AF. Possible effects of residual remanences have also been discussed [*Trindade et al.*, 2001]. *Yu and Dunlop* [2003] investigated decay-rate dependence of ARM in magnetite and report that for SD and PSD grains the ARM intensity is higher for slower decay rates, whereas for MD grains it is higher for faster decay rates. Since this may also affect AARM fabrics, it is advisable to report decay rates in future AARM studies. Sadly, decay rates have only been reported in one of the 82 AARM studies cited in this paper. The AF range over which the DC field is applied determines which subpopulations of grains, defined by their coercivities, are given an ARM. Most commonly, the bias field is applied over an AF range of 0-100 mT, followed in popularity by 0-60 mT, but a number of other windows have been used, and in some studies they are not reported at all (Figure 1c-d). Note that these parameters are not necessarily constrained by the instrumentation available, as shown by a survey on laboratory instrumentation currently available in magnetic laboratories around the world, as well as possible and typically used experimental parameters (Figure 1 e-h). The survey was distributed via the gpmag, emrp, and latinmag e-mail lists in January and February 2018. One interesting outcome of the survey is that even though most published AARM results were obtained using a DC field of 0.1 mT, the majority of laboratories that answered our survey report using 0.05 mT DC fields.

Several studies have measured ApARMs over multiple AF windows, to capture the preferred orientations of distinct subpopulations of magnetite grains, defined by their grain size and shape [*Aubourg and Robion*, 2002; *Biedermann et al.*, 2019b; *Bilardello and Jackson*, 2014; *Cioppa and Kodama*, 2003; *Jackson et al.*, 1988; *Nakamura and Borradaile*, 2001; *Raposo and Berquo*, 2008; *Raposo et al.*, 2004; *Salazar et al.*, 2016; *Sun and Kodama*, 1992; *Trindade et al.*, 1999; *Trindade et al.*, 2001]. Using ApARMs, *Jackson et al.* [1989a] have shown that the degree of magnetic foliation in black shales from Kansas decreases with increasing coercivity, thus leading to the interpretation that coarser magnetite grains in these shales possess a stronger foliation than smaller grains. *Trindade et al.* [2001] report that both the AMS and low-coercivity AARM in their granitic and noritic samples describe the primary fabrics of large magnetite grains, whereas the high-coercivity AARMs are related to secondary processes like hydrothermal alteration. In sandstones from the western Makran accretionary prism (Iran) low- and high-coercivity ApARMs indicate different orientations of the magnetic foliation, related to different preferred orientations of coarse and fine grains [*Aubourg and Robion*, 2002]. Therefore, AARM is not only able to provide additional information because it records a different fabric than the AMS, but different ApARMs may be able to further distinguish between deformation stages or tectonic events on a finer scale (Figure 2). However, unless there is a specific interest in isolating sub-fabrics or to correct a

specific remanence component, most studies measure only one set of AARMs. Thus, as a community, we are missing an opportunity to identify distinct magnetic sub-fabrics on our samples, because ApARMs are so rarely measured. Hence, we were interested to determine whether multiple sub-fabrics are a common feature across a range of lithologies.

This study characterizes the variation of AARM and ApARM principal directions, degree and shape of the anisotropy with the coercivity window over which the (p)ARMs are imparted. Additionally, we describe the consequences of using smaller or larger coercivity windows. Measurements shown here were performed on a suite of rocks from various locations and with different mineralogies: Samples originate from layered intrusions, lava flows, ocean floor gabbros, sedimentary red beds, metamorphic rocks, and high-fired ceramics. The results presented here will help our understanding of the link between mineralogy, texture and remanence anisotropy, and demonstrate that coercivity-dependent remanence anisotropy is actually a common feature in a wide variety of rocks. Note that a detailed geologic interpretation of the fabrics in our rocks is beyond the scope of this study.

2 Materials and Methods

2.1 Samples

The samples used in this study cover a range of rock types, including igneous, metamorphic and sedimentary rocks, as well as archeological material (high-fired ceramics). The rationale for characterizing a variety of rock types and ceramics is to determine how frequently coercivity-dependent variations in remanence anisotropy are observed. A full sample description including the coercivity distribution of the rock types investigated is provided in *Biedermann et al.* [in review].

For the purpose of this study, we were mainly interested in the preferred orientation, geometry and chemical composition (Fe/Ti ratio) of iron oxides. The samples contain several oxides, including compositions in the hematite-ilmenite and magnetite-ulvöspinel solid solutions. Additional sulfides are present in some samples. Image analysis of thin section photographs and backscattered electron (BSE) images obtained on a JEOL JXA-8900R electron microprobe at the Department of Earth Sciences, University of Minnesota, indicate several oxide populations, distinct in their grain orientations, sizes, and geometries. The microprobe was operated at accelerating voltage of 10 keV, with a beam current of 12 nA and a focused beam. Additionally, elemental maps were obtained with a beam current of 30 nA, and 20 ms dwell time. These show different preferred orientations for inclusions of different sizes and compositions, suggesting that different populations of inclusions may correspond to different coercivity windows of A(p)ARMs (Figure 3). Awareness of such mineralogical complexity is important in interpreting magnetic fabric results.

2. 2 Susceptibility and anisotropy of susceptibility

Magnetic susceptibility and its anisotropy were measured on an AGICO MFK1-FA susceptibility bridge, operated at the instrument's standard settings of 200 A/m field and 976 Hz frequency. Full susceptibility tensors were calculated from measurements in three mutually perpendicular planes, or measuring directional susceptibility in 15 orientations [*Jelinek*, 1977; 1996]. Susceptibility is described by a second-order symmetric tensor with eigenvalues $k_1 \geq k_2 \geq k_3$, whose eigenvectors represent the principal susceptibility directions. The degree of anisotropy will be described here by $P = k_1/k_3$, and by the mean

deviatoric susceptibility $k' = \sqrt{((k_1 - k_{mean})^2 + (k_2 - k_{mean})^2 + (k_3 - k_{mean})^2)/3}$, where $k_{mean} = (k_1 + k_2 + k_3)/3$ is the mean susceptibility, and its shape by $U = (2 * k_2 - k_1 - k_3)/(k_1 - k_3)$ [*Jelinek*, 1981; 1984]. Whereas *P* is more commonly used to describe anisotropy degree, *k'* is better suited to compare the contributions of different sub-fabrics. All results will be shown in a sample coordinate system. *Hext* [1963]'s statistics were used to determine whether or not anisotropy is significant. When anisotropy was not significant (e13 > 26°), k is represented by an isotropic tensor with all diagonal elements equal to k_{mean}.

2. 3 Anisotropy of (partial) anhysteretic remanent magnetization (A(p)ARM)

The remanence anisotropy tensors measured for this study are the same as for *Biedermann et al.* [in review], and a full description of the method is provided there. We repeat here one note on terminology: we use ApARM to denote the anisotropy of pARM acquired in a window (AF_1, AF_2), where $AF_1 > AF_2$ and $AF_2 > 0$; AARM indicates anisotropy of remanence where $AF_2 = 0$, whether or not AF_1 is the maximum available field. The coercivity windows (0-20 mT, 20-50 mT, 50-100 mT, and 100-180 mT) were chosen based on a combination of the coercivity spectra across the sample collection, instrumental limitations, and practical considerations, e.g. that coercivity windows need to be large enough to obtain statistically significant data.

3 Results

3.1 Susceptibility and anisotropy of susceptibility

Mean susceptibilities cover the range from $5.9*10^{-8}$ m^3/kg to $4.0*10^{-5}$ m^3/kg over the entire sample collection (Figure 4). The degree of anisotropy varies from *P* = 1.01 to 1.59, and the mean deviatoric susceptibility *k'* varies over several orders of magnitude, between $9.3*10^{-10}$ m^3/kg and $5.2*10^{-6}$ m^3/kg. The AMS ellipsoids display a wide range of shapes, from *U* = -0.865 to U = 0.941. An overview of AMS data and summary of the typical ranges of these parameters, as well as the normalized principal susceptibilities, are reported in Table S1 (Supporting Information).

3.2 A(p)ARM

3.2.1 Variation of A(p)ARM with coercivity

An overview of all remanence anisotropy tensors for all samples is provided in *Biedermann et al.* [in review], and in Table S2 (Supporting Information). Here, we focus on how ApARMs and AARMs depend on the coercivity window over which the remanence was imparted. Principal directions, degree and shape of the A(p)ARM tensors may vary as a function of the coercivity window (Figures 5-7). ARM anisotropy is not significant in all windows for all specimens. Some specimens display significant anisotropy in discrete windows, but not in others. The overall AARM can be dominated by the anisotropy associated with a single window, or may be a superposition of the ApARMs of several windows. When the ApARMs in all windows are coaxial, they interfere positively to form a strong overall AARM. Conversely, when the principal directions of individual ApARMs have different orientations, they partly cancel each other, forming a weaker total AARM. This range of observations highlights the suitability of our sample collection to investigate numerous possible interactions between different ApARM sub-fabrics in defining the overall

AARM. Below we discuss for each sample group how A(p)ARMs vary across different coercivity windows, and how they superpose to form the overall AARM. For paleomagnetic applications, it is important to view the different magnetic tensors within the context of a sample's NRM demagnetization behavior.

3.2.1.1 Duluth Complex

Troctolites and gabbros from the Duluth Complex lose between 40 and 80% of their NRM at AF steps below 20 mT, followed by slower decay in higher AF fields. For three samples (NLMD_NTl_02_01_02_01, NLMD_NxG_01_01_03_01, _01_01_04_01), the NRM demagnetization behavior is directly reflected by the mean ARM acquired in each coercivity window. In a second group of samples (NLMD_NTl_01_01_02_01, _01_01_03_01, _01_01_03_02, NLMD_NxG_02_01_01_01, _02_01_02_01), the strongest mean ARM is acquired in the 20-50 mT coercivity range, even though this coercivity range is only responsible for 10-30% NRM loss.

In the first group $AARM_{0\text{-}20}$ shows a higher *k'* than any of the ApARMs (Figure 5a). Principal directions are different for the $AARM_{0\text{-}20}$ tensor than the ApARM tensors; these may correspond to the two oxide populations observed in thin section. All ApARMs are similar, but do not coincide. The minimum and intermediate axes of $AARM_{0\text{-}20}$ are rotated up to about 70° with respect to the corresponding axes of $ApARM_{20\text{-}50}$. $AARM_{0\text{-}50}$, $AARM_{0\text{-}100}$, and $AARM_{0\text{-}180}$, all spanning larger coercivity windows, are composite fabrics incorporating $AARM_{0\text{-}20}$ and the ApARMs observed in the higher coercivity windows. The orientations of the principal axes gradually rotate away from the $AARM_{0\text{-}20}$ principal directions and towards the $ApARM_{20\text{-}50}$, $ApARM_{50\text{-}100}$ and $ApARM_{100\text{-}180}$ principal axes as the coercivity window increases to incorporate higher fields.

In the second group, *k'* is also higher for $AARM_{0\text{-}20}$ than the ApARMs in all samples but one for which $ApARM_{20\text{-}50}$ is higher (Figure 5b). Principal directions appear more similar for $AARM_{0\text{-}20}$ and $ApARM_{20\text{-}50}$ than for the first group, and the principal directions of the AARMs spanning several coercivity windows plot in-between those two. The AARMs, $AARM_{0\text{-}50}$, $AARM_{0\text{-}100}$, $AARM_{0\text{-}180}$, all have similar *k'*, which is higher than any *k'* of the individual coercivity contributions, indicating positive interference of all grain sizes.

3.2.1.2 Bushveld Complex

Small losses in NRM are observed below 20 mT AF in specimens from the Bushveld Complex, but the largest part of the NRM is lost in fields > 40 mT AF. These specimens had been demagnetized to 120 mT or 140 mT, and 25%-50% of the initial NRM remained after the end of the demagnetization experiment. Remanence in these samples is not held by hematite or goethite, and therefore, this residual magnetization is thought to be held by grains of high-coercivity magnetite and titanomagnetite [*Feinberg et al.*, 2005]. This behavior is also reflected in the ARM results, i.e. the highest mean ARM is either carried by the 50-100 coercivity fraction (all BG1.xx samples), or the 100-180 mT coercivity fraction (all BG2.xx samples) (Figure 5c). The mean deviatoric susceptibility *k'* is highest for the 50-100 fraction (BG1.17A, BG1.23A, BG2.04A, BG2.07A, BG2.09A), or the 100-180 fraction (BG1.02, BG1.16A, BG2.05A). Both mean ARM and *k'* are minor or insignificant for $AARM_{0\text{-}20}$. For most samples, principal directions show one set of directions for $AARM_{0\text{-}20}$, a second set for $ApARM_{20\text{-}50}$ and $ApARM_{50\text{-}100}$, and a third for $ApARM_{100\text{-}180}$. An exception is BG2.07A, for which the $AARM_{0\text{-}20}$ and $ApARM_{20\text{-}50}$ directions are similar. The directions of the combined AARMs ($AARM_{0\text{-}50}$, $AARM_{0\text{-}100}$, and $AARM_{0\text{-}180}$) are mostly dominated by the $ApARM_{20\text{-}50}$ and $ApARM_{50\text{-}100}$ contributions.

The anisotropy is strongest for the full-spectrum $AARM_{0-180}$, followed by the contributing fractions $AARM_{0-100}$, $ApARM_{50-100}$, and $ApARM_{100-180}$. *k'* for $ApARM_{20-50}$ and $AARM_{0-50}$ are similar, each amounting to only 10%-20% of the *k'* for $AARM_{0-180}$.

3.2.1.3 Bjerkreim Sokndal Layered Intrusion

The igneous samples from Bjerkreim Sokndal can be divided into three groups based on their AF demagnetization and AARM behavior, which is related to differences in dominating ferromagnetic (*sensu lato*) mineralogy.

Samples in the first group (sites BK2015_24, _25, _28 and _49) are characterized by a strong NRM decay below 20 mT, followed by a weaker decay between 20-50 mT, often a second stronger decay between 50-100 mT, and a slower decay above 100 mT. Mean ARM as well as *k'* are strongest in the 0-20 mT window (Figure 5d), which also largely dominated the $AARM_{0-50}$, $AARM_{0-100}$ and $AARM_{0-180}$. For most of these samples, both the principal directions as well as the *k'* of the latter are very similar to that of $AARM_{0-20}$. $ApARM_{20-50}$, $ApARM_{50-100}$ and $ApARM_{100-180}$ show either similar, slightly rotated or entirely different orientation of principal axes as compared to $AARM_{0-20}$, but their contributions to the overall ARM anisotropy are small.

Samples of the second group (sites BK2015_27 and _31) show little change in NRM during AF demagnetization up to 50 mT, followed by stronger decreases in fields larger than 50 mT or larger than 100 mT. 10% to 25% of the NRM remains after the maximum demagnetizing field of 200 mT. The mean ARM acquired in each individual window increases for higher windows for all samples except one (Figure 5e). The mean deviatoric susceptibility either increases for progressive individual windows, or is similar in each window. All individual AARMs contribute to the combined AARMs, and the principal directions of $AARM_{0-50}$, $AARM_{0-100}$, and $AARM_{0-180}$ progressively move away from those of $AARM_{0-20}$ and towards those of $AARM_{0-180}$.

Samples from the remaining sites (BK2015_29, _30, and _40) either show an intermediate behavior between that of Group 1 and Group 2, or a large variation in behaviors between samples from the same site, some being more similar to Group 1, and others to Group 2.

3.2.1.4 Fogo Basalts

The basalt samples from Fogo lose most of their NRM at AFs <20 mT. This coercivity fraction can also acquire the largest mean ARM, but its anisotropy is only significant in 2 of 4 samples (Figure 6a). *k'* is similar for all coercivity fractions with significant anisotropy. In general, principal AARM directions are similar for all coercivity windows, individual and combined, but the observed $AARM_{0-50}$ has a distinct orientation in 3 out of 4 samples. The anisotropy of the measured $AARM_{0-100}$ and $AARM_{0-180}$ are not significant in any of the samples, but should be highest according to tensor addition of the A(p)ARMs in the individual windows. The strong remanences acquired by the Fogo basalts were at the upper limit of the instrument, and many measurements had to be discarded because of flux jumps. It is possible that the noise introduced by measuring at the instruments' limit masked the anisotropy of these samples. The strongest measurable anisotropy is observed for $AARM_{0-50}$.

3.2.1.5 Ocean floor gabbro

Ocean floor gabbros from the ODP735B drill core show a pronounced loss of NRM below 20 mT AF, or a steady decay up to 120 mT AF, the maximum field to which they were demagnetized. Up to 20% of initial NRM remains at 120 mT AF.

ApARM tensors and the degree of anisotropy for specific coercivity windows vary widely between samples. Mean ARM is largest in the 0-20 mT window in three samples (ODP735.042, ODP735.097, ODP735.159), and $AARM_{0\text{-}20}$ also displays the strongest *k'* for these samples (Figure 6b). Principal directions can be different for each A(p)ARM, and AARMs appear to be largely dominated by the orientation of $AARM_{0\text{-}20}$, with additional contributions from $ApARM_{20\text{-}50}$.

Mean ARM can also be highest for intermediate coercivity windows, i.e. either for $ApARM_{20\text{-}50}$ or $ApARM_{50\text{-}100}$. In these samples (e.g. sample ODP735.166, Figure 6c), *k'* is highest for intermediate or high coercivities, and principal axes can have similar orientations independent of the coercivity window, or show a wide spread. In general, $AARM_{0\text{-}180}$ and $AARM_{0\text{-}100}$ display the strongest *k'*, followed by $AARM_{0\text{-}50}$, and the ApARMs contribute varying amounts.

3.2.1.6 Thomson Slate

Those Thomson Slate samples that had not been demagnetized previously, show the strongest NRM decay at intermediate coercivities, i.e. in the 20-50, or the 50-100 mT windows. These are also the windows acquiring the strongest mean pARMs for all but one sample (TS4.7b has strongest mean pARM in 50-100 and 100-180 windows).

Only three samples show significant ApARMs in all coercivity windows. For two of these (TS9.9a and TS12.5a, Figure 6d), *k'* is highest for $ApARM_{50\text{-}100}$, and for the other (TS12.9) it is largest for $ApARM_{100\text{-}180}$. Principal susceptibility directions show a distinct orientation of $AARM_{0\text{-}20}$ axes for all of these samples. A smaller variation between the principal axes orientations of $ApARM_{20\text{-}50}$, $ApARM_{50\text{-}100}$, and $ApARM_{100\text{-}180}$ is observed for the two samples whose ApARM is strongest for intermediate coercivities. Each coercivity window seems to have distinct principal axes orientations for the sample with highest *k'* for $ApARM_{100\text{-}180}$. The principal directions for the AARMs appear to be dominated by the principal axes orientations of the highest-coercivity ApARM that is contributing.

Only small amounts of ferromagnetic material are present in these samples. Thus, it is difficult to establish whether the insignificant A(p)ARMs for certain coercivity windows in the other samples are related to the fact that no A(p)ARM is carried by these grain sizes, or whether the variation due to noise is higher than that related to anisotropy.

3.2.1.7 Mauch Chunk Formation

Mauch Chunk red bed samples show an initial NRM loss in AFs < 5 mT, followed by a slow decay up to 100 mT, and a slightly faster decay between 100-200 mT. More than 50% of the NRM remains after demagnetization to 200 mT, which is the maximum field our AF demagnetizer can reach. Even though the largest NRM loss is observed in the 100-180 mT window, mean ARMs in each window are approximately equal (Figure 6e).

The mean deviatoric susceptibility *k'* is by far highest in the high-coercivity window, i.e. $ApARM_{100\text{-}180}$. Two samples exhibit no significant $ApARM_{20\text{-}50}$ (MC17_4, MC17_5a), and one sample has no significant anisotropy either in the 0-20 nor the 20-50 mT window

(MC17_5b). Principal directions show up to three distinct orientations, one for $AARM_{0\text{-}20}$, a second for $ApARM_{20\text{-}50}$, $ApARM_{50\text{-}100}$, $AARM_{0\text{-}50}$ and $AARM_{0\text{-}100}$, and a third for $ApARM_{100\text{-}180}$, and $AARM_{0\text{-}180}$. Comparing the AARM degrees to the ApARMs reveals that *k'* is largest for $AARM_{0\text{-}180}$, which is very similar to $k'_{100\text{-}180}$, and far higher than *k'* for $AARM_{0\text{-}100}$ and $AARM_{0\text{-}50}$.

3.2.1.8 High-fired ceramic material

The ceramic samples lose most of their NRM below 60 mT, followed by a slower decay. The coercivity distributions vary between specimens. The samples acquire anhysteretic remanence mainly in the 20-50 mT window, followed by the 0-20 mT window (Figure 6f). For three out of the four samples, $k'_{0\text{-}20}$ is highest, and for one sample (KS2378_D), the strongest anisotropy is observed in the same window that carries the highest mean pARM, i.e. 20-50 mT. Principal directions are similar for most AARMs and ApARMs.

3.2.1.9 Summary

A comparison of anisotropy parameters for all samples in each group shows that the coercivity fractions dominating remanence anisotropy are consistent within some but not all lithologies. Consistent localities include the Duluth Complex, Bushveld Complex, and Mauch Chunk Formation (Figure 7). Conversely, the ocean floor gabbro and rocks from the Bjerkreim Sokndal intrusion show comparatively larger variations between different specimens. Two observations common to all localities are that (1) the degree of AMS can be significantly higher or lower than the remanence anisotropy, and hence AMS is not a good proxy for remanence anisotropy, and (2) the degree of remanence anisotropy and its orientation can vary largely with coercivity in all samples investigated here.

4 Discussion

4.1 Comparison between AMS and AARM tensors

Comparing the principal directions and mean deviatoric susceptibility *k'* for AMS and the different AARM tensors can help identify which minerals or grain size fractions contribute to the AMS, and thus may help in the structural interpretation of both the AMS and AARM tensors.

For the Duluth Complex samples, the AMS principal directions most closely relate to, but do not coincide with, those of the $AARM_{0\text{-}20}$. *k'* of the AMS is smaller than *k'* of any of the AARMs and $ApARM_{20\text{-}50}$, but similar to $ApARM_{50\text{-}100}$ and $ApARM_{100\text{-}180}$. Similarly, the AMS principal directions for most samples from Bjerkreim Sokndal are near those of either their $AARM_{0\text{-}20}$ or other AARMs. In these samples, the *k'* of the AMS is lower than, or similar to, the *k'* of the AARMs. These observations indicate that the low-coercivity grains responsible for $AARM_{0\text{-}20}$ may contribute significantly to the AMS. When the AMS degree is lower than that of the AARM, this may be explained by a contribution of paramagnetic minerals, or MD magnetite with lower anisotropy. It is also possible that AMS and AARM are controlled by different carrier minerals, which have experienced the same deformation, giving rise to similar orientations of the anisotropy ellipsoids. The progressive rotation of minimum and intermediate axes of AMS, $AARM_{0\text{-}20}$, $AARM_{0\text{-}50}$, $AARM_{0\text{-}100}$, $AARM_{0\text{-}180}$ for e.g. NLMD_NxG_01_01_04_01 could be interpreted as a deformation affecting large paramagnetic grains as well as larger isometric ferromagnetic (i.e. low-coercivity) grains in a different way from the smaller or more elongated high-coercivity grains (cf. Figures 2, 3).

Samples from the Bushveld Complex have an AMS k' an order of magnitude lower than $k'_{0\text{-}180}$, indicating a high ARM/susceptibility ratio and strong anisotropy. Four samples (BG1.xx) show AMS_{min} // $AARM_{max}$, which may be indicative of inverse fabrics as observed in SD magnetite [*Ihmlé et al.*, 1989; *Rochette*, 1988; *Rochette et al.*, 1999], or MD grains with a different fabric from the remanence-carrying grains. The relationship between AMS and AARM directions is less straightforward for the remaining four samples (BG2.xx), in which AMS_{min} appears at a ca. 20° - 50° angle to $AARM_{max}$. Assuming that SD magnetite partly contributes to the AMS and AARM of these samples, its effect on AMS is smaller than on the AARM. Possible reasons for this behavior are that susceptibility and remanence are fundamentally different properties, especially for SD grains whose AMS exhibits inverse fabrics, and therefore the SD contribution to the AMS will counteract that of the larger magnetite grains. Secondly, the AMS is diluted by the contribution of more isotropic paramagnetic minerals. However, the AMS and AARM tensors for BG2.xx are not coaxial and do not show the characteristics typical for inverse fabrics, ruling out SD grains as the major source of the AMS. Several minerals contribute to the AMS, resulting in complex fabrics.

The principal AMS axes in the Fogo basalts appear unrelated to any set of principal A(p)ARM axes. Additionally, k'_{AMS} is about an order of magnitude smaller than k'_{AARM}. Because AMS is very weak, there are large confidence angles (errors) around the principal axes directions, so that differences in directions have to be interpreted with caution. AMS could also be influenced by the paramagnetic minerals, however, separation of fabrics based on high-field measurements [*Ferré et al.*, 2004; *Kelso et al.*, 2002; *Martín-Hernández and Hirt*, 2001; 2004; *Martín-Hernández and Ferré*, 2007] would be necessary to assess this effect.

For the ocean floor gabbros, the AMS principal axes can be related to either the orientation of $AARM_{0\text{-}20}$, or $ApARM_{50\text{-}100}$, or they are oblique to any of the A(p)ARM tensors. For all these samples, AMS is weaker than most of the AARMs. This indicates that although ferromagnetic grains may contribute to the AMS, it is largely influenced by paramagnetic grains with lower anisotropy than the ferromagnetic grains.

Thomson Slate samples show a unique behavior in that their k'_{AMS} is consistently higher than any AARM measured on the same sample. This confirms that the AMS is controlled mainly by paramagnetic minerals, as has been reported in previous studies [*Johns et al.*, 1992; *Sun et al.*, 1995]. Principal directions of AMS and AARMs are sometimes sub-parallel, but can also be oblique. This is consistent with the findings of Sun et al [1995] that the AARM mainly reflects the primary bedding and compaction fabric of the magnetite particles, whereas the AMS is dominated by the paramagnetic chlorite that defines the cleavage produced by later metamorphism and tectonic deformation. The changes in principal-axis orientations across coercivity windows indicate variable overprinting of the primary fabric in different particle size fractions of magnetite.

For the Mauch Chunk red bed samples, the k'_{AMS} is again lower than any k'_{AARM}. The principal directions of AMS and $AARM_{0\text{-}20}$ or $AARM_{0\text{-}50}$ are often sub-parallel, particularly for the minimum axes. AMS principal axes are oblique to the $AARM_{0\text{-}180}$ or $ApARM_{100\text{-}180}$, which are the A(p)ARMs with strongest k'. The low-coercivity AARMs and AMS are likely dominated by the small amounts of magnetite present in these samples, whereas the high-coercivity A(p)ARMs may record some of the hematite contribution. Hematite occurs in the

Mauch Chunk Formation as both pigmentary and specular grains and therefore, while stronger isothermal remanent magnetizations are necessary to fully activate the higher coercivity detrital grains, AARMs may be sufficient to (partly) activate the pigment [*Bilardello*, 2015].

In the ceramic specimens, the AMS and AARM tensors are sub-parallel, with the remanence anisotropy being stronger than the AMS. Hence, AMS is likely carried by ferromagnetic grains.

4.2 Variation of remanence anisotropy tensors with coercivity

Numerous studies have shown differences in principal directions or anisotropy degree between AMS and remanence anisotropy, or between various types of remanence anisotropies, e.g. AARM, AIRM, and ATRM [*Bilardello and Jackson*, 2014; *Borradaile and Jackson*, 2010; *Selkin et al.*, 2000]. Some initial studies on ApARMs have also shown that fabrics can be dramatically different for ApARMs imparted over different coercivity windows [*Aubourg and Robion*, 2002; *Biedermann et al.*, 2019b; *Jackson et al.*, 1989a; *Trindade et al.*, 2001]. Here, AARMs in a range of coercivitiy windows have been systematically investigated for a selection of samples from different rock types and localities, in order to cover a broad spectrum of A(p)ARM behaviors. A(p)ARMs generally differ when they have been imposed over different coercivity windows, and these differences can be expressed as changes in principal directions, anisotropy degree, or the shape of the AARM ellipsoid.

Figure 8 shows a schematic overview of the observed characteristics of ApARMs and AARMs across our sample suite:

(1) AARMs can be dominated by the contribution of minerals in one specific coercivity window, or by a combination of the individual AARMs in several windows. Additionally, if several grain size fractions/AARM tensors contribute, their individual anisotropies can interfere constructively or destructively. This is similar to results obtained from AMS studies, i.e. AMS can be predominantly carried by one mineral, or by a combination of several minerals. In the latter case, the individual contributions to AMS can add up or partially cancel each other out [*Biedermann et al.*, 2015]. A more complete picture of the complex superposition is obtained by measurement of the anisotropies of different coercivity fractions.

(2) The mean deviatoric susceptibility k' of the AARM can increase, decrease or vary non-monotonically when the coercivity window is increased. Because of this, P-values of AARMs can increase or decrease as the coercivity window becomes larger. When k' increases with increasing window size, the contributions of the constituent sub-populations are likely sub-parallel. Conversely, when it decreases, the tensors of each sub-population are likely to be oriented differently, or may even be mutually inverse.

(3) The grain fraction acquiring the strongest mean ARM does not necessarily carry the highest anisotropy. This is analogous to a similar observation common to AMS studies, where magnetite often dominates the bulk susceptibility, but contributes little (or not at all) to the AMS [*Borradaile*, 1987; B*orradaile et al.*, 1985/86; *Hirt et al.*, 1995; *Hounslow*, 1985; *Rochette*, 1987; *Rochette and Vialon*, 1984; *Rochette et al.*, 1992]. Only by measuring ApARMs for a set of coercivity windows can we begin to identify the principal components of composite anisotropy.

(4) By virtue of (1) and (3), the AARM as measured over the entire coercivity range in a sample may not be representative of the remanence anisotropy exhibited by the minerals that carry the (largest part of) the NRM. In some cases (e.g., the Mauch Chunk red beds), the main NRM carriers may reside in a coercivity range which is higher than what may be reached with AARM [Biedermann et al., 2019a]. However, even when the NRM is carried by magnetite, and the ARM coercivity spectrum matches that of NRM, the full-spectrum AARM may be a composite of subfabrics with different orientations and/or degrees of anisotropy, and not ideal for correcting the NRM for inclination shallowing or anisotropic NRM acquisition [Biedermann et al., 2109b]. This can only be evaluated by measuring ApARM over a set of coercivity windows.

It has long been recognized that the low-field AMS, being a superposition of magnetic anisotropies of paramagnetic, diamagnetic and ferromagnetic (*sensu lato*) grains and their alignment, may be hard to interpret in the case of complex fabrics. Similarly, the present study shows that a bulk AARM, measured over the entire coercivity range of a specimen, may not be an adequate description of remanence anisotropy. Different sub-populations of grains may each possess a distinct fabric, and their anisotropies can interfere positively or negatively. Separating the ApARM fabrics carried by sub-populations of grains, as defined by their coercivities, can provide additional information in fabric interpretation studies [*Aubourg and Robion*, 2002; *Jackson et al.*, 1989a; *Nakamura and Borradaile*, 2001; *Trindade et al.*, 1999; *Trindade et al.*, 2001], and forms the basis for more complete anisotropy corrections in paleomagnetic studies [*Biedermann et al*, 2019b].

In this study, sub-populations of grains are defined by their coercivities. Coercivity can be related to mineralogy (e.g. hematite generally has a higher coercivity than magnetite), grain size (small stable SD grains have higher coercivity than larger MD grains), grain shape (elongated grains have higher coercivity), and chemical composition (e.g. Ti content) of the remanence carriers. Initial microprobe and image analysis results suggest that different orientations of iron-titanium oxide inclusions exsolved within silicate minerals may show distinct Fe/Ti ratios. Such varying degrees of Ti-substitution are likely linked to different rates of diffusion along particular crystallographic axes in the host silicate, and may help explain the changes in ApARM directions associated with different coercivity windows (cf Figures 2, 3, and 5-8). Detailed single-crystal work is still needed to fully discriminate between the different magnetic grain characteristics and their relationships to ApARM anisotropies in these samples. In any case, the results presented here indicate that the commonly measured $AARM_{0\text{-}100}$, although it targets a smaller fraction of grains than low-field AMS, may still reflect a composite fabric that is hard to interpret in terms of structural or tectonic processes. Specifically targeting a subset of the remanence-carrying grains with ApARMs may reveal multiple fabric contributions, which can in turn be related to several tectonic events. Because coercivity-dependent fabrics have here been observed for a range of igneous, metamorphic and sedimentary rocks, we believe that partial remanence anisotropies have large potential in disentangling the strain and deformation fields in structural and tectonic studies.

5 Conclusions

We have shown that for a large range of geologic settings and rock types, as well as archaeological material, remanence anisotropy tensors strongly depend on the coercivity window over which the remanence was applied. The orientation of principal axes, as well as

the degree and shape of anisotropy vary widely for different ApARMs imposed on the same sample. Therefore, bulk AARMs also vary depending on the size of the AF window over which the DC field was applied. Similar to AMS being carried by a superposition of anisotropy contributions from different minerals, these coercivity-dependent variations in A(p)ARM can be related to the presence of several sub-populations of grains – defined by their grain size, shape or composition – having different fabrics. Therefore, the anisotropy degree *P* of the AARMs can increase or decrease when the DC bias field is applied over a larger AF range.

Even though it has been shown that ApARMs are a powerful tool to investigate e.g. early versus late fabrics in structural and tectonic studies, most published results are simply $AARM_{0\text{-}100}$ tensors. Because of the variation of AARM parameters and principal direction with coercivity as reported here, we strongly encourage researchers to carefully choose their experimental parameters, measure ApARMs rather than one AARM, and report the experimental settings in future studies on fabrics of remanence-carrying grains, as well as when performing anisotropy corrections in paleomagnetic and archaeomagnetic studies. Most rocks have experienced multiple stages of deformation and alteration, and ApARMs measured over different coercivity windows are one of the only methods available for characterizing the fabrics associated with each of these stages. Thus, ApARMs are poised to play a central role in the reconstruction of deformation and alteration histories in future research.

Acknowledgments

The authors wish to thank the community for answering our AARM experimental parameters survey. Anette von der Handt is thanked for help with the microprobe measurements. We are grateful to Maxwell Brown, Suzanne McEnroe, Peter Hudleston, and Lisa Tauxe for discussions on magnetic fabrics related to different sample sets included in this study. We also appreciate the efforts of František Hrouda and an anonymous reviewer, as well as the editor and associate editor, in helping to improve the initial version of this paper. This study was conducted under Swiss National Science Foundation project 167608, and measurements were performed at the Institute for Rock Magnetism (IRM) at the University of Minnesota. The IRM is a US National Multi-user Facility supported through the Instrumentation and Facilities program of the National Science Foundation (Earth Sciences Division), and funding from the University of Minnesota. This is IRM publication #1810. The full set of data can be downloaded from the Supplementary Material, or the MagIC database, doi: 10.7288/V4/MAGIC/16724.

References

Aubourg, C., and P. Robion (2002), Composite ferromagnetic fabrics (magnetite, greigite) measured by AMS and partial AARM in weakly strained sandstones from western Makran, Iran, *Geophysical Journal International*, *151*, 729-737.

Biedermann, A. R., K. Kunze, A. S. Zappone, and A. M. Hirt (2015), Origin of magnetic fabric in ultramafic rocks, *IOP Conference Series: Materials Science and Engineering*, *82*(1).

Biedermann, A. R., M. Jackson, D. Bilardello, and S. A. McEnroe (2017), Effect of magnetic anisotropy on the natural remanent magnetization in the MCU IVe' layer of the Bjerkreim Sokndal Layered Intrusion, Rogaland, Southern Norway, *Journal of Geophysical Research – Solid Earth*.

Biedermann, A. R., F. Heidelbach, M. Jackson, D. Bilardello, and S. A. McEnroe (2016), Magnetic fabrics in the Bjerkreim Sokndal Layered Intrusion, Rogaland, southern Norway: Mineral sources and geological significance, *Tectonophysics*, *688*, 101-118.

Biedermann, A. R., M. Jackson, M. D. Stillinger, D. Bilardello, and J. M. Feinberg (in review), Anisotropy of full and partial anhysteretic remanence across different rock types: 1. Are partial anhysteretic remanence anisotropy tensors additive?, *This journal*

Biedermann, A. R., D. Bilardello, M. Jackson, and J. Feinberg (2019a), Anisotropy of (partial) isothermal remanent magnetization: Variation with DC field, and additivity, *Geophysical Journal International*, *218*(2), 1428-1441, doi: 10.1093/gji/ggz234.

Biedermann, A.R., D. Bilardello, M. Jackson, L. Tauxe, and J. M. Feinberg (2019b), Grain-size-dependent remanence anisotropy and its implications for paleodirections and paleointensities - proposing a new approach to anisotropy corrections, *Earth and Planetary Science Letters*

Bijaksana, S., and J. P. Hodych (1997), Comparing remanence anisotropy and susceptibility anisotropy as predictors of paleomagnetic inclination shallowing in turbidites from the Scotian Rise, *Phys. Chem. Earth*, *22*(1-2), 189-193.

Bilardello, D. (2015), Isolating the anisotropy of the characteristic remanence-carrying hematite grains: a first multispecimen approach, *Geophysical Journal International 202(2)*, 695-712.

Bilardello, D., and M. J. Jackson (2014), A comparative study of magnetic anisotropy measurement techniques in relation to rock-magnetic properties, *Tectonophysics*, *629*, 39-54.

Bilardello, D., and K. P. Kodama (2009), Measuring remanence anisotropy of hematite in red beds: anisotropy of high-field isothermal remanence magnetization (hf-AIR), *Geophysical Journal International 178(3)*, 1260-1272.

Borradaile, G. (1987), Anisotropy of magnetic susceptibility: rock composition versus strain, *Tectonophysics*, *138*, 327-329.

Borradaile, G., J. Mothersill, D. Tarling, and C. Alford (1985/86), Sources of magnetic susceptibility in a slate, *Earth and Planetary Science Letters*, *76*(3-4), 336-340.

Borradaile, G. J. (2001), Magnetic fabrics and petrofabrics: their orientation distributions and anisotropies, *Journal of Structural Geology*, *23*(10), 1581-1596.

Borradaile, G. J., and F. Lagroix (2000), Thermal enhancement of magnetic fabrics in high grade gneisses, *Geophysical Research Letters*, *27*(16), 2413-2416.

Borradaile, G. J., and F. Lagroix (2001), Magnetic fabrics reveal Upper Mantle Flow fabrics in the Troodos Ophiolite Complex, Cyprus, *Journal of Structural Geology*, *23*, 1299-1317.

Borradaile, G. J., and D. Gauthier (2003), Interpreting anomalous magnetic fabrics in ophiolite dikes, *Journal of Structural Geology*, *25*(2), 171-182.

Borradaile, G. J., and B. S. Almqvist (2008), Correcting distorted paleosecular variation in late glacial lacustrine clay, *Physics of the Earth and Planetary Interiors*, *166*, 30-43.
Borradaile, G. J., and M. Jackson (2010), Structural geology, petrofabrics and magnetic fabrics (AMS, AARM, AIRM), *Journal of Structural Geology*, *32*(10), 1519-1551.
Borradaile, G. J., R. A. Stewart, and T. Werner (1993), Archean uplift of a subprovince boundary in the Canadian Shield, revealed by magnetic fabrics, *Tectonophysics*, *227*, 1-15.
Borradaile, G. J., F. Lagroix, and D. King (1998), Tilting and transpression of an Archaean anorthosite in northern Ontario, *Tectonophysics*, *293*(3-4), 239-254.
Borradaile, G. J., T. Werner, and F. Lagroix (1999a), Magnetic fabrics and anisotropy-controlled thrusting in the Kapuskasing Structural Zone, Canada, *Tectonophysics*, *302*, 241-256.
Borradaile, G. J., P. W. Fralick, and F. Lagroix (1999b), Acquisition of anhysteretic remanence and tensor subtraction from AMS isolates true palaeocurrent grain alignments, in *Palaeomagnetism and Diagenesis in Sediments*, edited by D. H. Tarling and P. Turner, pp. 139-145, Geological Society Special Publications, London, UK.
Borradaile, G. J., F. Lagroix, and D. Trimble (2001), Improved isolation of archeomagnetic signals by combined low temperature and alternating field demagnetization, *Geophysical Journal International*, *147*, 176-182.
Borradaile, G. J., F. Lagroix, T. D. Hamilton, and D.-A. Trebilcock (2010), Ophiolite Tectonics, Rock Magnetism and Paleomagnetism, Cyprus, *Surveys in Geophysics*, *31*, 285-359.
Calvin, P., V. C. Ruiz-Martinez, J. J. Villalain, A. M. Casas-Sainz, and B. Moussaid (2017), Emplacement and Deformation of Mesozoic Gabbros of the High Atlas (Morocco): Paleomagnetism and Magnetic Fabrics, *Tectonics*.
Chadima, M., P. Pruner, S. Slechta, T. Grygar, and A. M. Hirt (2006), Magnetic fabric variations in Mesozoic black shales, Northern Siberia, Russia: Possible paleomagnetic implications, *Tectonophysics*, *418*, 145-162.
Cioppa, M. T., and K. P. Kodama (2003), Environmental magnetic and magnetic fabric studies in Lake Waynewood, northeastern Pennsylvania, USA: Evidence for changes in watershed dynamics, *Journal of Paleolimnology*, *29*, 61-78.
Cogné, J.P. (1987), TRM deviations in anisotropic assemblages of multidomain magnetites, Geophysical Journal of the Royal Astronomical Society, 90, 1013–1023.
Cogné, J. P., and H. Perroud (1988), Anisotropy of magnetic susceptibility as a strain gauge in the Flamanville granite, NW France, Physics of the Earth and Planetary Interiors, 51, 264-270.
Collombat, H., P. Rochette, and D. V. Kent (1993), Detection and correction of inclination shallowing in deep sea sediments using the anisotropy of anhysteretic remanence, *Bull. Soc. geol. France*, *164*, 103-111.
de Wall, H., and H.-U. Worm (1993), Field dependence of magnetic anisotropy in pyrrhotite: effects of texture and grain shape, *Physics of the Earth and Planetary Interiors*, *76*, 137-149.
Evans, M. A., M. T. Lewchuk, and R. D. Elmore (2003), Strain partitioning of deformation mechanisms in limestones: examining the relationship of strain and anisotropy of magnetic susceptibility (AMS), *Journal of Structural Geology*, *25*(25), 1525-1549.
Feinberg, J.M., G.R. Scott, P.R. Renne, and H.-R. Wenk (2005), Exsolved magnetite inclusions in silicates: Features determining their remanence behavior, Geology, 33, 513-516.

Ferré, E. C., F. Martin-Hernandez, C. Teyssier, and M. Jackson (2004), Paramagnetic and ferromagnetic AMS in migmatites: Measurements in high and low fields and kinematic implications, *Geophysical Journal International*, *157*, 1119-1129.

Fuller, M. (1963), Magnetic anisotropy and paleomagnetism, *J. Geophys. Res.*, *68*, 293–309.

Gattacceca, J., and P. Rochette (2002), Pseudopaleosecular variation due to remanence anisotropy in a pyroclastic flow succession, *Geophysical Research Letters*, *29*(8), 127-121 - 127-124.

Gattacceca, J., P. Rochette, and M. Bourot-Denise (2003), Magnetic properties of a freshly fallen LL ordinary chondrite: the Bensour meteorite, *Physics of the Earth and Planetary Interiors*, *140*, 343-358.

Gaudreau, E., D. Schneider, F. Lagroix, E. Cossette, and B. Grasemann (2017), Controls and implications of anisotropy across a strain gradient within granodiorite, Serifos, Greece, *Journal of Geodynamics*, *105*, 11-26.

Hext, G. R. (1963), The estimation of second-order tensors, with related tests and designs, *Biometrika*, *50*(3/4), 353-373.

Hirt, A. M., K. F. Evans, and T. Engelder (1995), Correlation between magnetic anisotropy and fabric for Devonian shales on the Appalachian Plateau, *Tectonophysics*, *247*, 121-132.

Hirt, A. M., A. R. Biedermann, and N. S. Mancktelow (2014), Magnetic study of a late Alpine dike crosscutting the regional foliation, *Tectonophysics*, *629*, 250-259.

Hirt, A. M., W. Lowrie, W. S. Clendenen, and R. Kligfield (1993), Correlation of strain and the anisotropy of magnetic susceptibility in the Onaping Formation: evidence for a near-circular origin of the Sudbury Basin, *Tectonophysics*, *225*, 231-254.

Hodych, J. P., and S. Bijaksana (1993), Can remanence anisotropy detect paleomagnetic inclination shallowing due to compaction? A case study using cretaceous deep-sea limestones, *Journal of Geophysical Research*, *98*(B12), 22429-22441.

Hodych, J. P., S. Bijaksana, and R. Pätzold (1999), Using magnetic anisotropy to correct for paleomagnetic inclination shallowing in some magnetite-bearing deep-sea turbidites and limestones, *Tectonophysics*, *307*, 191-205.

Hounslow, M. W. (1985), Magnetic fabric arising from paramagnetic phyllosilicate minerals in mudrocks, *Journal of the Geological Society*, *142*, 995-1006.

Housen, B. A., and van der Pluijm, B.A. (1991), Slaty cleavage development and magnetic anisotropy fabrics, *Journal of Geophysical Research*, *96*(B6), 9937-9946.

Hrouda, F., B. Henry, and G. J. Borradaile (2000), Limitations of tensor subtraction in isolating diamagnetic fabrics by magnetic anisotropy, *Tectonophysics*, *322*, 303-310.

Hrouda, F. (2002), The use of the anisotropy of magnetic remanence in the resolution of the anisotropy of magnetic susceptibility into its ferromagnetic and paramagnetic components, *Tectonophysics*, 347(4), 269-281.

Ihmlé, P. F., A. M. Hirt, W. Lowrie, and D. Dietrich (1989), Inverse magnetic fabric in deformed limestones of the Morcles Nappe, Switzerland, *Geophysical Research Letters*, *16*(12), 1383-1386.

Issachar, R., T. Levi, S. Marco, and R. Weinberger (2015), Anisotropy of magnetic susceptibility in diamagnetic limestones reveals deflection of the strain field near the Dead Sea Fault, northern Israel, *Tectonophysics*, *656*, 175-189.

Issachar, R., T. Levi, S. Marco, and R. Weinberger (2018), Separation of diamagnetic and paramagnetic fabrics reveals strain directions in carbonate rocks, *Journal of Geophysical Research - Solid Earth*.

Jackson, M., and L. Tauxe (1991), Anisotropy of magnetic susceptibility and remanence: Developments in the characterization of tectonic, sedimentary, and igneous fabric, *Reviews of Geophysics*, *29*, 371-376.

Jackson, M., D. Sprowl, and B. B. Ellwood (1989a), Anisotropies of partial anhysteretic remanence and susceptibility in compacted black shales: Grain-size and composition-dependent magnetic fabric, *Geophysical Research Letters*, *16*, 1063-1066.
Jackson, M., W. Gruber, J. Marvin, and S. K. Banerjee (1988), Partial anhysteretic remanence and its anisotropy: applications and grainsize-dependence, *Geophysical Research Letters*, *15*, 440-443.
Jackson, M., G. J. Borradaile, P. Hudleston, and S. Banerjee (1993), Experimental deformation of synthetic magnetite-bearing calcite sandstones: effects on remanence, bulk magnetic properties and magnetic anisotropy, *Journal of Geophysical Research*, *98*, 383-401.
Jackson, M., J. P. Craddock, M. Ballard, R. van der Woo, and C. McCabe (1989b), Anhysteretic remanent magnetic anisotropy and calcite strains in Devonian carbonates from the Appalachian Plateau, New York, *Tectonophysics*, *161*, 43-53.
Jelinek, V. (1977), The statistical theory of measuring anisotropy of magnetic susceptibility of rocks and its application, edited, p. 88, Geofyzika Brno, Brno, Czechoslovakia.
Jelinek, V. (1981), Characterization of the magnetic fabric of rocks, *Tectonophysics*, *79*, T63-T67.
Jelinek, V. (1984), On a mixed quadratic invariant of the magnetic susceptibility tensor, *Journal of Geophysics - Zeitschrift fur Geophysik 56*, 58-60.
Jelinek, V. (1996), Measuring anisotropy of magnetic susceptibility on a slowly spinning specimen - basic theory, edited, AGICO Print No 10, Brno, Czechoslovakia.
Johns, M. K., M. J. Jackson, and P. J. Hudleston (1992), Compositional control of magnetic anisotropy in the Thomson formation, east-central Minnesota, *Tectonophysics*, *210*, 45-58.
Kapper, L., F. Donadini, V. Serneels, E. Tema, A. Goguitchaichvili, and J. J. Morales (2017), Reconstructing the geomagnetic field in West Africa: first absolute intensity results from Burkina Faso, *Nature*, *7*.
Kelso, P. R., B. Tikoff, M. Jackson, and W. Sun (2002), A new method for the separation of paramagnetic and ferromagnetic susceptibility anisotropy using low field and high field methods, *Geophysical Journal International*, *151*(2), 345-359.
Kiss, D., E. Marton, and A. K. Tokarski (2016), An integrated paleomagnetic and magnetic anisotropy study of the Oligocene flysch from the Dukla nappe, Outer Western Carpathians, Poland, *Geologica Carpathica*, *67*(6), 595-605.
Kissel, C., C. Laj, A. Mazaud, and T. Dokken (1998), Magnetic anisotropy and environmental changes in two sedimentary cores from the Norwegian Sea and the North Atlantic, *Earth and Planetary Science Letters*, *164*, 617-626.
Kligfield, R., W. Lowrie, and W. D. Dalziel (1977), Magnetic susceptibility anisotropy as a strain indicator in the Sudbury Basin, Ontario, *Tectonophysics*, *40*, 287-308.
Kligfield, R., W. H. Owens, and W. Lowrie (1981), Magnetic susceptibility anisotropy, strain, and progressive deformation in Permian sediments from the Maritime Alps (France), *Earth and Planetary Science Letters 55*, 181-189.
Kodama, K. P. (1997), A successful rock magnetic technique for correctng paleomagnetic inclination shallowing: Case study of the Nacimiento Formation, New Mexico, *Journal of Geophysical Research - Solid Earth*, *102*(B3), 5193-5205.
Kodama, K. P. (2009), Simplification of the anisotropy-based inclination correction technique for magnetite- and haematite-bearing rocks: a case study of the Carboniferous Glenshaw and Mauch Chunk Formations, North America, *Geophysical Journal International*, *176*, 467-477.

Kodama, K. P., and A. Mowery (1994), Paleomagnetism of the Sassamansville diabase, Newark Basin, southeastern Pennsylvania: Support for Middle Jurassic high-latitude paleopoles for North America, *Geological Society of America Bulletin*, *106*, 952-961.

Kodama, K. P., and M. J. Dekkers (2004), Magnetic anisotropy as an aid to identifying CRM and DRM in red sedimenetary rocks, *Studia Geophysica Et Geodaetica*, *48*, 747-766.

Kon, S., N. Nakamura, Y. Nishimura, K. Goto, and D. Sugawara (2017), Inverse magnetic fabric in unconsolidated sandy event deposits in Kiritappu Marsh, Hokkaido, Japan, *Sedimentary Geology*, *349*, 112-119.

Lagroix, F., and G. J. Borradaile (2000a), Tectonics of the circum-Troodos sedimentary cover of Cyprus, from rock magnetic and structural observations, *Journal of Structural Geology*, *22*, 453-469.

Lagroix, F., and G. J. Borradaile (2000b), Magnetic fabric interpretation complicated by inclusions in mafic silicates, *Tectonophysics*, *325*, 207-225.

Li, Y.-X., and K. P. Kodama (2005), Assessing thermal effects on magnetic fabrics of sedimentary rocks: Results from synthetic and natural samples, *Geophysical Research Letters*, *32*, L04314.

Lycka, R. (2017), A Systematic Comparison of the Anisotropy of Magnetic Susceptibility (AMS) and Anisotropy of Remanence (ARM) Fabrics of Ignimbrites: Examples from the Quaternary Bandelier Tuff, Jemez Mountains, New Mexico and Miocene Ignimbrites near Gold Point, Nevada, UT Dallas.

Mamtani, M. A., S. Piazolo, R. O. Greiling, A. Kontny, and F. Hrouda (2011), Process of magnetite fabric development during granite deformation, *Earth and Planetary Science Letters*, *308*, 77-89.

Martín-Hernández, F., and A. M. Hirt (2001), Separation of ferrimagnetic and paramagnetic anisotropies using a high-field torsion magnetometer, *Tectonophysics*, *337*(3-4), 209-221.

Martín-Hernández, F., and A. M. Hirt (2004), A method for the separation of paramagnetic, ferrimagnetic and haematite magnetic subfabrics using high-field torque magnetometry, *Geophysical Journal International*, *157*(1), 117-127.

Martín-Hernández, F., and E. C. Ferré (2007), Separation of paramagnetic and ferrimagnetic anisotropies: A review, *Journal of Geophysical Research-Solid Earth*, *112*(B3).

McCabe, C., M. Jackson, and B. B. Ellwood (1985), Magnetic anisotropy in the Treton limestone: results of a new technique, anisotropy of anhysteretic suscecptibility, *Geophysical Research Letters*, *12*, 333-336.

Molinek, F. R., and D. Bilardello (2018), Application of an anisotropy-based correction to relative paleointensity estimates of experimentally deposited sediments, *Geochemistry Geophysics Geosystems*.

Nakamura, N., and G. J. Borradaile (2001), Strain, anisotropy of anhysteretic remanence, and anisotropy of magnetic susceptibility in a slaty tuff, *Physics of the Earth and Planetary Interiors*, *125*, 85-93.

Nowaczyk, N. R. (2003), Detailed study on the anisotropy of magnetic susceptibility of arctic marine sediments, *Geophysical Journal International*, *152*(2), 302-317.

Oliva-Urcia, B., J. C. Larrasoana, E. L. Pueyo, A. Gil, P. Mata, J. M. Parés, A. M. Schleicher, and O. Pueyo (2009), Disentangling magnetic subfabrics and their link to deformation processes in cleaved sedimentary rocks from the Internal Sierras (west central Pyrenees, Spain), *Journal of Structural Geology*, *31*(2), 163-176.

Pignotta, G. S., and K. Benn (1999), Magnetic fabric of the Barrington Passage pluton, Meguma Terrane, Nova Scotia: a two-stage fabric history of syntectonic emplacement, *Tectonophysics*, *307*, 75-92.

Ponte, J. M., E. Font, C. Veiga-Pires, C. Hillaire-Marcel, and B. Ghaleb (2017), The effect of speleothem surface slope on the remanent magnetic inclination, *Journal of Geophysical Research - Solid Earth*, *122*(6), 4143-4156.

Potter, D. K. (2004), A comparison of anisotropy of magnetic remanence methods - a user's guide for application to paleomagnetism and magnetic fabric studies, in *Magnetic Fabric: Methods and Applications*, edited by F. Martin-Hernandez, C. M. Lüneburg, C. Aubourg and M. Jackson, pp. 21-35, Geological Society Special Publications, London, UK.

Raposo, M. I. B., and M. S. D'Agrella-Filho (2000), Magnetic fabrics of dike swarms from SE Bahia State, Brazil: their significance and implications for Mesoproterozoic basic magmatism in the Sao Francisco Craton, *Precambrian Research*, *99*, 309-325.

Raposo, M. I. B., and T. S. Berquo (2008), Tectonic fabric revealed by AARM of the proterozoic mafic dike swarm in the Salvador city (Bahia State): Sao Francisco Craton, NE Brazil, *Physics of the Earth and Planetary Interiors*, *167*, 179-194.

Raposo, M. I. B., and M. C. P. Gastal (2009), Emplacement mechanism of the main granite pluton of the Lavras do Sul intrusive complex, South Brazil, determined by magnetic anisotropies, *Tectonophysics*, *466*(1-2), 18-31.

Raposo, M. I. B., I. McReath, and M. S. D'Agrella-Filho (2006), Magnetic fabrics, rock magnetism, cathodoluminescence and petrography of apparently undeformed Bambui carbonates from Sao Francisco Basin (Minas Gerais State, SE Brazil): An integrated study, *Tectonophysics*, *418*(1-2), 14.

Raposo, M. I. B., M. S. D'Agrella-Filho, and J. P. P. Pinese (2007), Magnetic fabrics and rock magnetism of Archaean and Proterozoic dike swarms in the southern Sao Francisco Craton, Brazil, *Tectonophysics*, *443*, 53-71.

Raposo, M. I. B., L. F. Pressi, and V. de Assis Janasi (2012), Magnetic fabrics and their relationship with the emplacement of the Piracaia pluton, SE Brazil, *International Journal of Earth Science (Geologische Rundschau)*, *101*, 773-786.

Raposo, M. I. B., C. O. Drukas, and M. A. S. Basei (2014), Deformation in rocks from Itajai basin, Southern Brazil, revealed by magnetic fabrics, *Tectonophysics*, *629*, 290-302.

Raposo, M. I. B., A. O. Chaves, P. Lojkasek-Lima, M. S. D'Agrella-Filho, and W. Teixeira (2004), Magnetic fabrics and rock magnetism of Proterozoic dike swarm from the southern Sao Francisco Craton, Minas Gerais State, Brazil, *Tectonophysics*, *378*, 43-63.

Rochette, P. (1987), Magnetic susceptibility of the rock matrix related to magnetic fabric studies, *Journal of Structural Geology*, *9*, 1015-1020.

Rochette, P. (1988), Inverse magnetic fabric in carbonate-bearing rocks, *Earth and Planetary Science Letters*, *90*, 229-237.

Rochette, P., and P. Vialon (1984), Development of planar and linear fabrics in Dauphinois shales and slates (French Alps) studied by magnetic anisotropy and its mineralogical control, *Journal of Structural Geology*, *6*(1/2), 33-38.

Rochette, P., M. Jackson, and C. Aubourg (1992), Rock magnetism and the interpretation of anisotropy of magnetic susceptibility, *Reviews of Geophysics*, *30*(3), 209-226.

Rochette, P., C. Aubourg, and M. Perrin (1999), Is this magnetic fabric normal? A review and case studies in volcanic formations, *Tectonophysics*, *307*, 219-234.

Sagnotti, L., F. Speranza, A. Winkler, M. Mattei, and R. Funiciello (1998), Magnetic fabric of clay sediments from the external northern Apennines (Italy), *Physics of the Earth and Planetary Interiors*, *105*, 73-93.

Salazar, C. A., C. Bustamante, and C. J. Archanjo (2016), Magnetic fabric (AMS, AAR) of the Santa Marta batholith (northern Colombia) and the shear deformation along the Caribbean Plate margin, *Journal of South American Earth Sciences*, *70*, 55-68.

Selkin, P. A., J. S. Gee, L. Tauxe, W. P. Meurer, and A. J. Newell (2000), The effect of remanence anisotropy on paleointensity estimates: a case study from the Archean Stillwater Complex, *Earth and Planetary Science Letters*, *183*, 403-416.

Soriano, C., E. Beamud, M. Garces, and M. H. Ort (2016), 'Anomalous' magnetic fabrics of dikes in the stable single domain/superparamagnetic threshold, *Geophysical Journal International*, *204*, 1040-1059.

Stephenson, A., S. Sadikun, and D. K. Potter (1986), A theoretical and experimental comparison of the anisotropies of magnetic susceptibility and remanence in rocks and minerals, *Geophysical Journal of the Royal Astronomical Society*, *84*, 185-200.

Stillinger, M.D., J.M. Feinberg, and E. Frahm (2015), Refining the archaeomagnetic dating curve for the Near East: new intensity data from Bronze Age ceramics at Tell Mozan, Syria, *Journal of Archaeological Science*, 53, 345-355.

Sun, W., P. J. Hudleston, and M. Jackson (1995), Magnetic and petrographic studies in the multiply deformed Thomson Formation, east-central Minnesota, *Tectonophysics*, *249*, 109-124.

Sun, W. W., and K. P. Kodama (1992), Magnetic anisotropy, scanning electron microscopy, and X ray pole figure goniometry study of inclination shallowing in a compacting clay-rich sediment, *Journal of Geophysical Research - Solid Earth*, *97*(B13), 19599-19615.

Tema, E. (2009), Estimate of the magnetic anisotropy effect on the archaeomagnetic inclination of ancient bricks, *Physics of the Earth and Planetary Interiors*, *176*, 213-223.

Trindade, R. I. F., M. I. B. Raposo, M. Ernesto, and R. Siqueira (1999), Magnetic susceptibility and partial anhysteretic remanence anisotropies in the magnetite-bearing granite pluton of Tourao, NE Brazil, *Tectonophysics*, *314*, 443-468.

Trindade, R. I. F., J.-L. Bouchez, O. Bolle, A. Nédélec, A. Peschler, and F. Poitrasson (2001), Secondary fabrics revealed by remanence anisotropy: methodological study and examples from plutonic rocks, *Geophysica Journal International*, *147*(2), 310-318.

Viegas, L. G. F., C. J. Archanjo, and A. Vauchez (2013), Fabrics of migmatites and the relationships between partial melting and deformation in high-grade transpressional shear zones: The Espinho Branco anatexite (Borborema Province, NE Brazil), *Journal of Structural Geology*, *48*, 45-56.

Werner, T., and G. J. Borradaile (1996), Paleoremanence dispersal across a transpressed Archean terrain: deflection by anisotropy of by late compression?, *Journal of Geophysical Research*, *101*, 5531-5545.

Yokoyama, E., R. I. F. Trindade, C. Lana, C. R. Souza Filho, D. Baratoux, Y. R. Marangoni, and E. Tohver (2012), Magnetic fabric of Araguainha complex impact structure (Central Brazil): Implications for deformation mechanisms and central uplift formation, *Earth and Planetary Science Letters*, *331-332*, 347-359.

Yu, Y., and D. J. Dunlop (2003), Decay-rate dependence of anhysteretic remanence: Fundamental origin and paleomagnetic applications, *Journal of Geophysical Research*, *108*(B12).

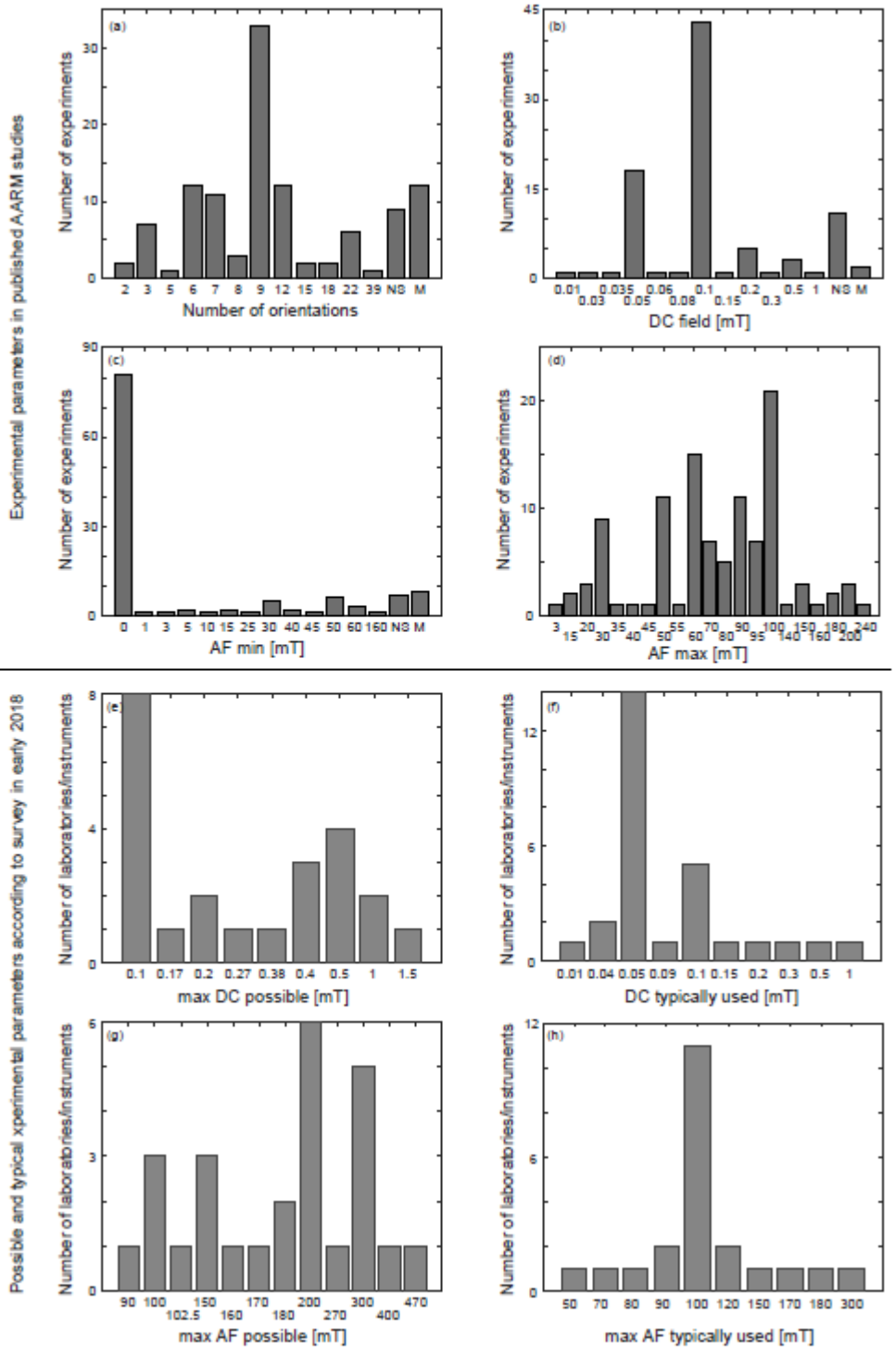

Figure 1: (a-d) Overview of number of remanences imposed, DC fields strength, and AF ranges over which the DC fields are applied in published studies including AARM measurements. (e-h) AF and DC ranges that are possible and typically used in rock and paleomagnetic laboratories, according to a survey distributed via the gpmag, emrp, and latinmag e-mail lists in early 2018.

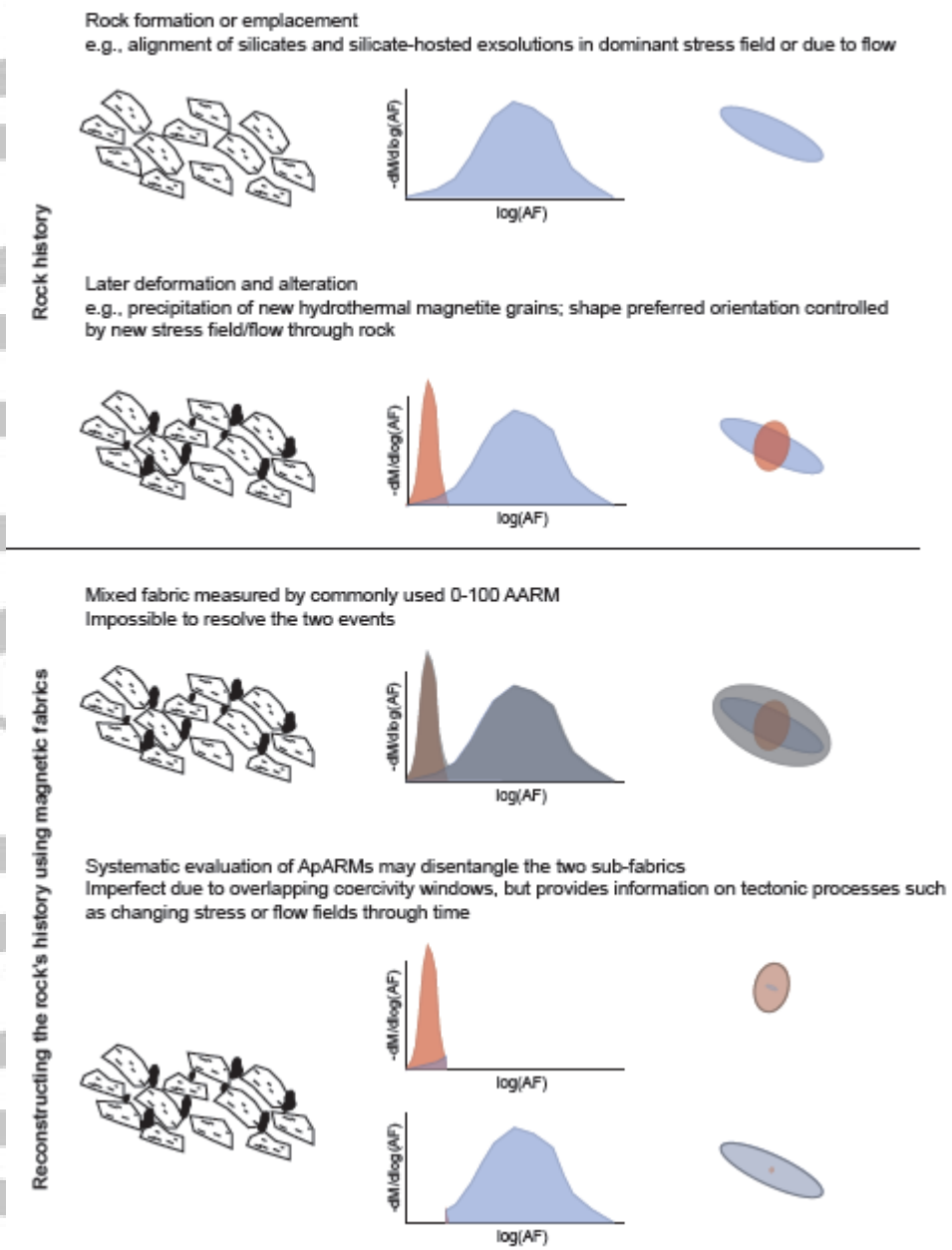

Figure 2: Schematic overview of AARM and ApARM measurements on a rock which contains multiple grain sub-population due to its tectonic and geologic history. Mineral populations (left column), corresponding coercivity spectra present in the rock and targeted by measurement (middle column), and contribution of magnetic sub-fabrics to measurements (right column). AARM targets all remanence-carrying grains, whereas ApARMs specifically capture the sub-fabrics of grain sub-populations within specific coercivity windows. Hence, ApARMs have the potential to further subdivide contributions to magnetic fabrics than is possible with comparing AMS (all grains) to AARM (remanence-carrying grains). Note that ApARMs do not provide information on the timing of events, but they allow us to characterize different events.

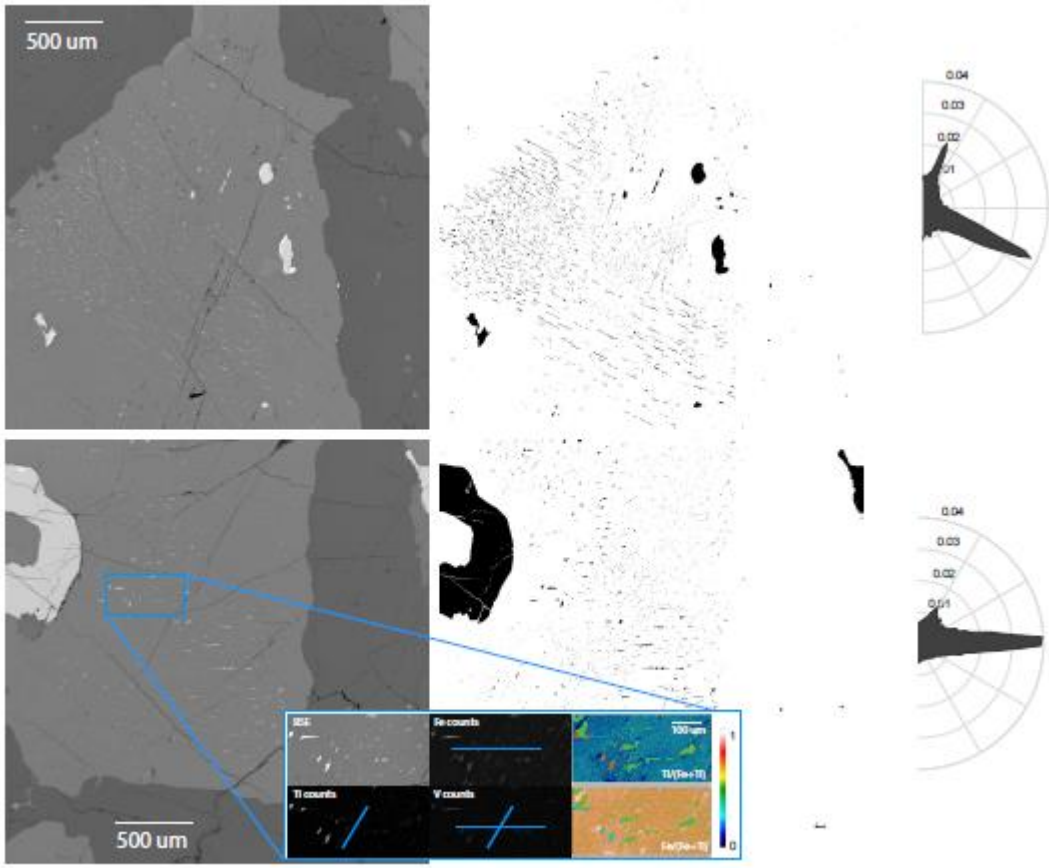

Figure 3: BSE images, image analysis of Fe oxide grains, and Fe, Ti, and V elemental maps, as well as Fe/(Fe+Ti) and Ti/(Fe+Ti) ratios for Duluth Complex sample NLMD_NxG_01_01_04_01. Blue lines on the element maps indicate preferred orientations of particles high in specific elements. Polar plots show long-axis orientation distributions for each BSE image. Note that there are several distinct preferred orientations of oxides, and that they tend to vary with grain size.

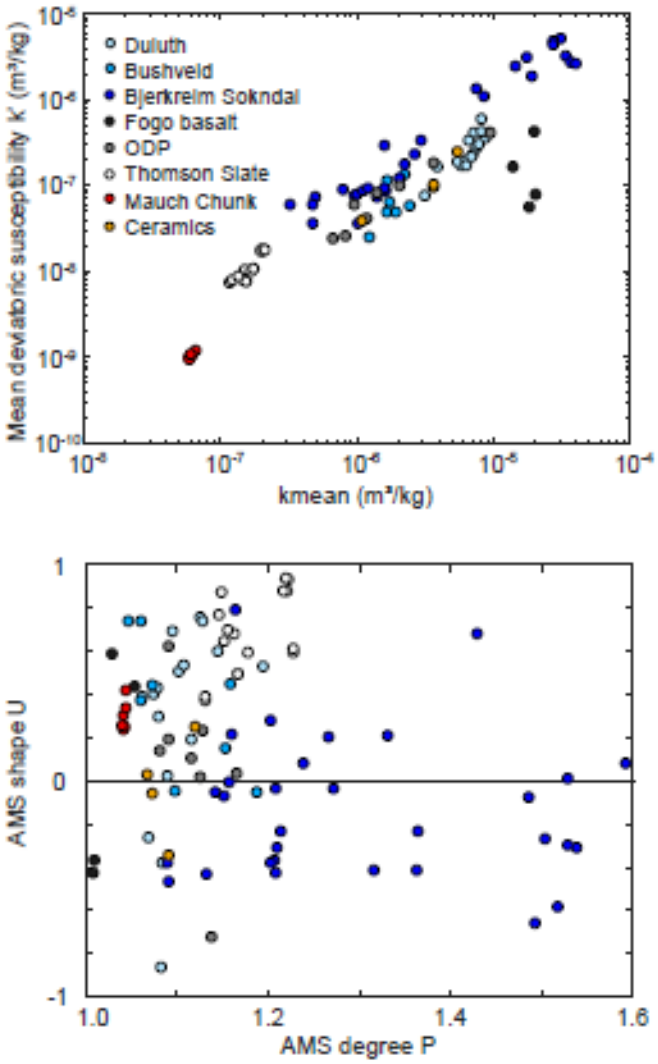

Figure 4: Summary of AMS results for each sample group.

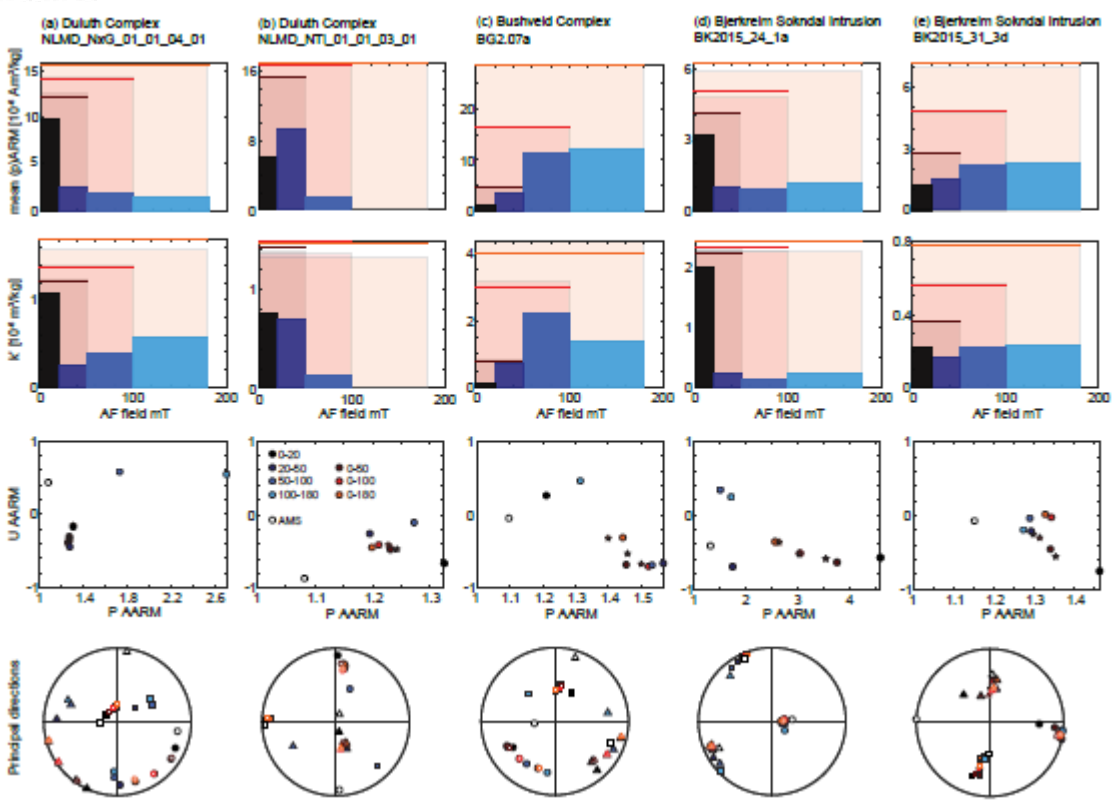

Figure 5: Mean (p)ARM, anisotropy parameters and principal directions for selected samples from layered intrusions. Colored boxes indicate the mean (p)ARM and k' in the respective windows. Dotted lines represent the parameters calculated by addition of ApARM tensors in the respective windows. For P-U plots, the circles indicate measured parameters, and stars represent parameters calculated by tensor addition from the ApARMs (see Biedermann et al. [in review] *for a full discussion of ApARM additivity). For principal directions, solid squares, triangles, and circles are the measured maximum, intermediate and minimum directions, and open symbols refer to the principal directions of corresponding calculated AARMs. Results are only plotted when anisotropy is significant at the 95% level. All parameters, and principal directions can change depending on the coercivity window. Note that the coercivity fraction carrying the largest mean ARM is not necessarily the same as that carrying the highest anisotropy.*

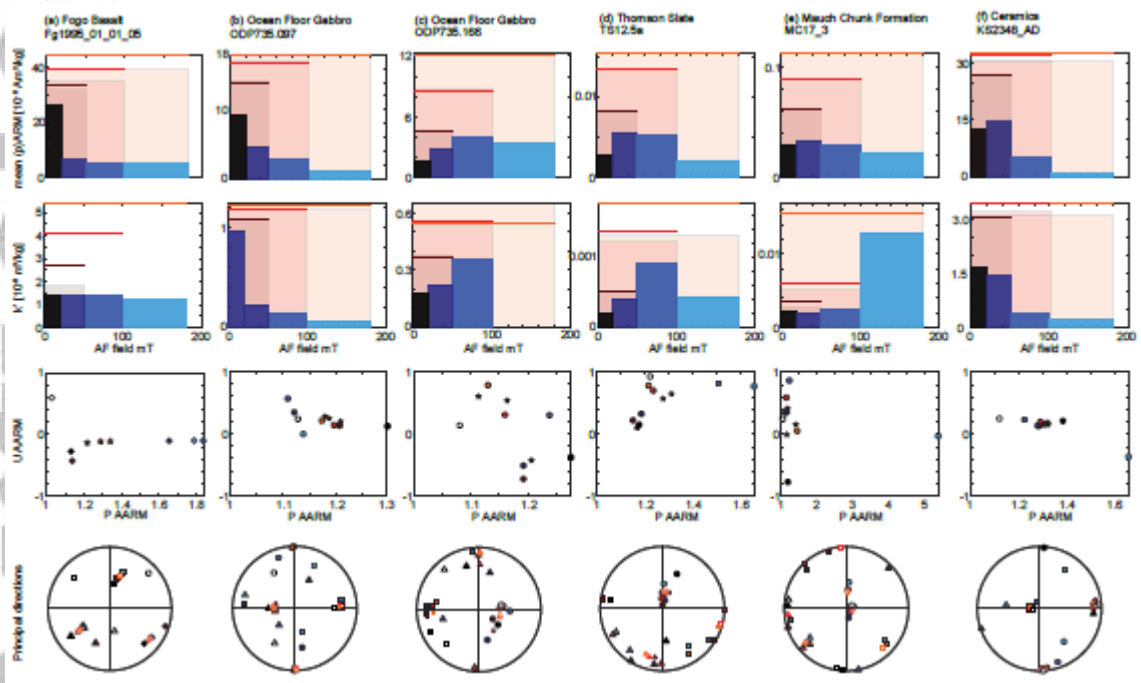

Figure 6: Mean (p)ARM, anisotropy parameters and principal directions for selected basalt, gabbro, metamorphic, sedimentary and ceramic samples. Cf Figure 5 for a full legend.

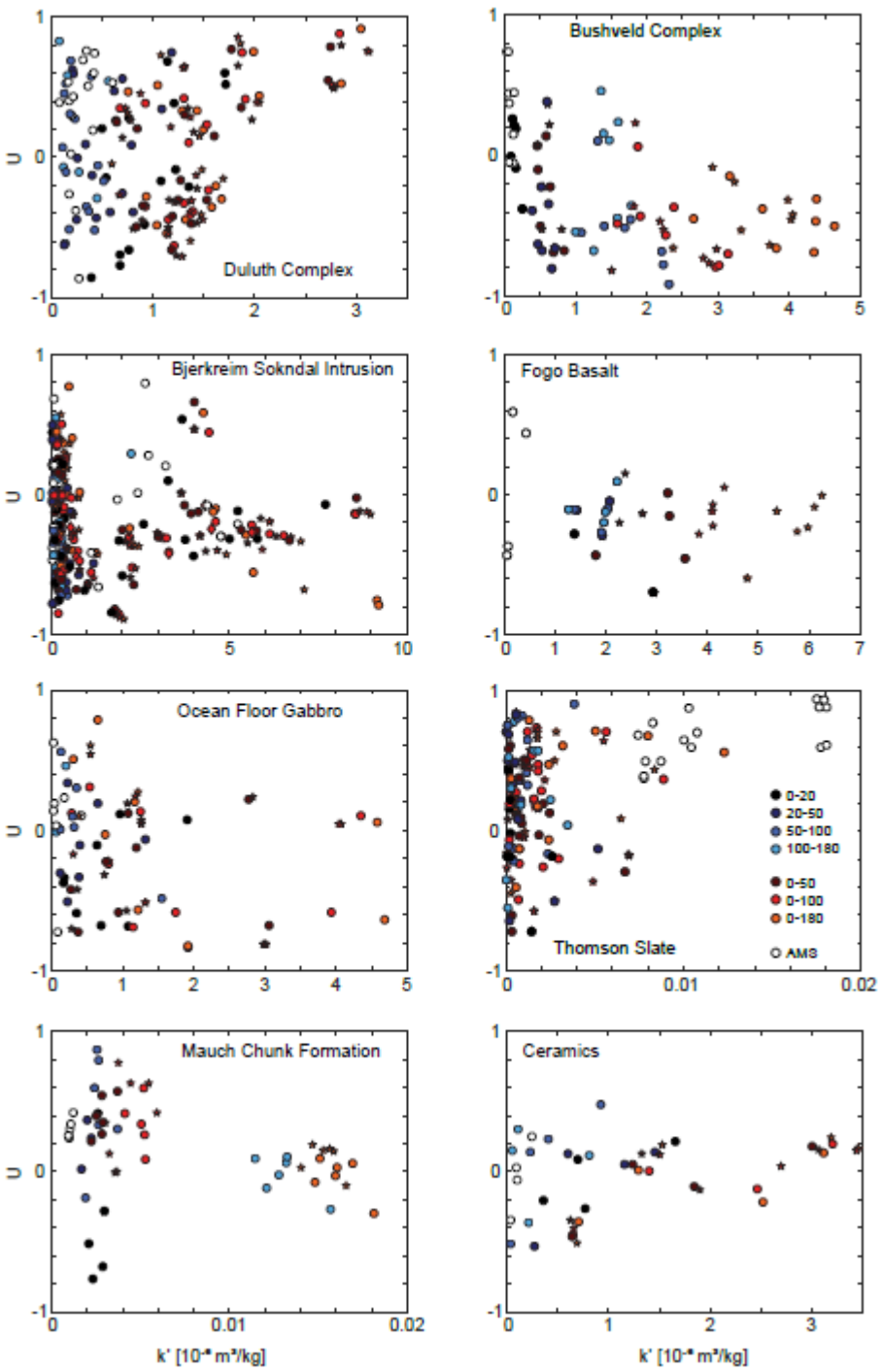

Figure 7: Overview of ApARM and AARM degree of anisotropy and shape as a function of coercivity window, in comparison to AMS parameters. Note how the overall AARM is dominated by different (combinations of) ApARMs in each rock type, and that there is generally more variability in U for rocks and coercivity windows with low k' values. Circles represent measured data, and stars are parameters calculated from tensor addition.

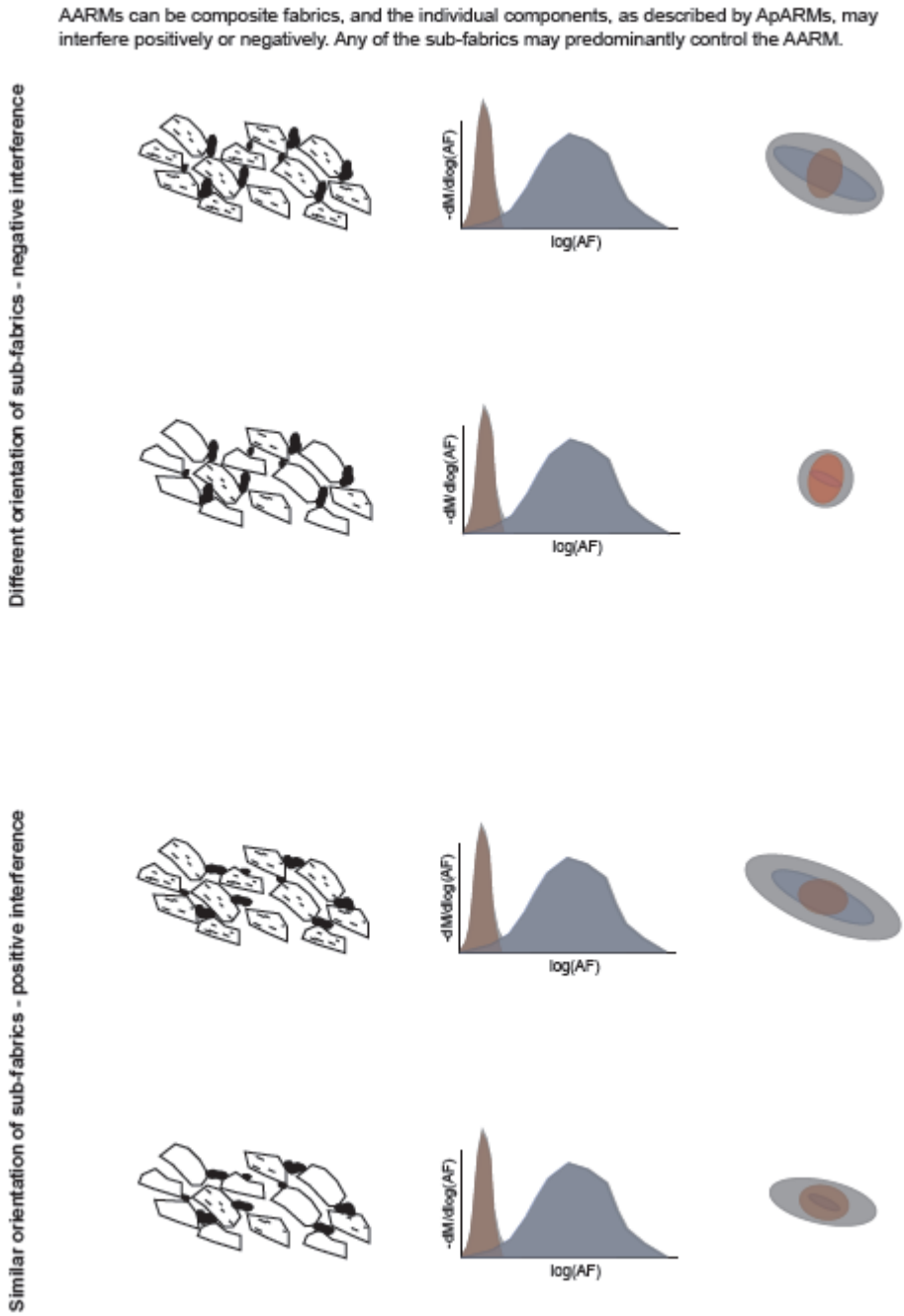

Figure 8: Interplay between the partial remanence anisotropies carried by multiple sub-populations of grains with different orientation relationships. Note that the overall AARM, being a superposition of several sub-fabrics potentially related to different tectonic events, may not reflect the orientation, degree, nor shape of anisotropy corresponding to the specific event. Hence, strain ellipsoids or deformation patterns interpreted based on AARMs may be incorrect. This is especially the case for multiple contributions that interfere negatively. ApARMs, on the other hand, can resolve the anisotropies associated with each event, and hence allow a more robust tectonic interpretation.